Comput. Methods Appl. Mech. Engrg. 200 (2011) 3011–3025

Contents lists available at ScienceDirect

Comput. Methods Appl. Mech. Engrg.

journal homepage: www.elsevier.com/locate/cma

Variational formulations for surface tension, capillarity and wetting

Gustavo C. Buscaglia *, Roberto F. Ausas

Instituto de Ciências Matemáticas e de Computação, Universidade de São Paulo, Av. do Trabalhador Sãocarlense 400, 13560-970 São Carlos, SP, Brazil
Instituto Nacional de Ciência e Tecnologia em Medicina Assistida por Computação Científica, Brazil

ARTICLE INFO

Article history:
Received 23 March 2011
Received in revised form 1 June 2011
Accepted 7 June 2011
Available online 17 June 2011

Keywords:
Surface tension
Marangoni force
Capillarity
Virtual-work principle
Surface gradient
Laplace-Beltrami operator

ABSTRACT

The interest in the simulation of flows with significant surface tension effects has grown significantly in recent years. This has been driven by the substantial advances made in the measurement and manufacturing of microscopic systems, since at small length scales surface phenomena are dominant. In this article, surface tension, capillarity and wetting effects are discussed in terms of the virtual–work principle and shape sensitivity, starting from first principles and arriving at variational formulations that are adequate for numerical treatment (by finite elements, for example). To make the exposition self-contained, some elements of differential geometry are recalled using a formulation that is fully in Cartesian coordinates and may thus be more friendly to readers not familiar with covariant derivatives. All necessary results are proved in this Cartesian formulation. Several numerical examples computed with a finite element/level set formulation are used to illustrate this challenging physical problem.

1. Introduction

The physics of surface tension, capillarity and wetting/dewetting phenomena is a very vast and active field of research for which a classical reference is the work of de Gennes and coworkers [1], while an update of the state of the art can be found in the article by Bonn et al. [2]. Informally speaking, surface tension appears whenever two immiscible fluids (A and B) are in contact, and is a consequence of the increased energy of the molecules of A (respectively, B) at the interface, as compared to those comfortably surrounded by identical neighbors at the bulk of fluid A (respectively, B).

Remark 1.1. Of course, depending on the pair A–B it may well happen that the molecules of A prefer to have some B-molecules around them rather than just A-molecules, but in this case the fluids would be miscible.

Over the years, a large volume of information has been published about the *numerical simulation of flows with interfaces*, of which review articles can be found [3–8]. These works consider either a passive interface or a capillary one, in which surface tension forces have been accounted for. However, capillary forces are introduced axiomatically, with little or no discussion of their physical and mechanical interpretation.

On the other hand, there is a growing interest in microscopic flows with quite complex interfaces. Textured, superhydrophobic and electrically modifiable surfaces have already entered microfluidic technologies [9–11], and the study and manipulation of complex colloids and biological interfaces is now within reach [12–14]. Successful numerical modeling of interfaces of such complexity cannot be performed without mechanical intuition and understanding. In fact, current research in elastic and geometric biomembranes is fundamentally based on energy considerations [15–21].

The plan for this article is to analyze the energetics of capillary phenomena from the viewpoint of the virtual–work principle, so as to translate the well-established physics (see, e.g., [1]) into a language more familiar to practitioners of computational mechanics. For this purpose, we first focus on a variational derivation of the virtual work $\mathcal{P}_\Gamma$ associated with the deformation of the interface Γ, which is the only difference with respect to the classical Stokes problem when Γ is closed, and then extend the analysis to problems with contact lines, in which as we will see both $\mathcal{P}_\Gamma$ and $\mathcal{P}_{\partial\Omega}$ play crucial roles. The derivation purposedly contains all required mathematical proofs in a seldom used but very practical framework that does not require covariant differentiation [22]. Along the analysis, connections to previous mathematical and numerical formulations are made, so as to discuss current practices from the proposed viewpoint, and some challenging open problems are identified.

2. Mathematical setting

Of the many surface-tension-related phenomena, we deliberately focus here on those involving two incompressible Newtonian

* Corresponding author at: Instituto de Ciências Matemáticas e de Computação, Universidade de São Paulo, Av. do Trabalhador Sãocarlense 400, 13560-970 São Carlos, SP, Brazil.
E-mail addresses: gustavo.buscaglia@icmc.usp.br, gustavo.buscaglia@gmail.com (G.C. Buscaglia), rfausas@gmail.com (R.F. Ausas).

0045-7825/$ - see front matter © 2011 Elsevier B.V. All rights reserved.
doi:10.1016/j.cma.2011.06.002

fluids at scales small enough for inertial and gravitational effects to be negligible. We consider the flow of these fluids in a domain Ω which for simplicity is assumed bounded by a rigid, impenetrable solid (its boundary is denoted by $\partial\Omega$, also assumed smooth). The domain Ω splits into two subdomains, Ω_+ occupied by fluid A and Ω_- occupied by fluid B. The interface between Ω_+ and Ω_- is denoted by Γ, which is assumed to be a smooth surface that can either be closed or have a boundary $\partial\Gamma$ at which there exists fluid/fluid/solid contact (the well-known "contact line"). A sketch of the geometrical setting in two dimensions can be seen in Fig. 1, but the three-dimensional situation ($d = 3$) is assumed throughout this article.

It is also assumed that there is no slip between the fluids at the interface, so that a global velocity field $\mathbf{u} \in (H^1(\Omega))^d$ can be defined. A global pressure $p \in L^2(\Omega)$ is also defined, and the viscosity $\mu(\mathbf{x})$ is taken as $\mu_A(\mathbf{x})$ if $\mathbf{x} \in \Omega_+$ and as $\mu_B(\mathbf{x})$ if $\mathbf{x} \in \Omega_-$.

Introducing the spaces

$$W \doteq \left\{\mathbf{w} \in (H^1(\Omega))^d | \mathbf{w} \cdot \check{\mathbf{n}} = 0 \text{ at } \partial\Omega\right\}, \tag{1}$$

$$Q \doteq L^2(\Omega)/\mathbb{R}, \tag{2}$$

the variational formulation of the problem reads: Find $(\mathbf{u}, p) \in W \times Q$ such that

$$\int_\Omega 2\mu D\mathbf{u} : D\mathbf{w} d\Omega - \int_\Omega p\nabla \cdot \mathbf{w} d\Omega = \int_\Omega \mathbf{b} \cdot \mathbf{w} d\Omega + \mathcal{P}_{\partial\Omega}(\mathbf{w}) + \mathcal{P}_\Gamma(\mathbf{w}), \tag{3}$$

$$\int_\Omega q\nabla \cdot \mathbf{u} d\Omega = 0 \tag{4}$$

for all $(\mathbf{w}, q) \in W \times Q$.

Above, $\mathbf{b} \in (L^2(\Omega))^d$ is a body force introduced for completeness, which may arise for example from electrophoretic effects, but will not be discussed. Because W admits tangential movement of the fluid with respect to $\partial\Omega$, a linear form $\mathcal{P}_{\partial\Omega} : W \to \mathbb{R}$ has been introduced expressing the virtual work at the boundary. Similarly, $\mathcal{P}_\Gamma$ is a linear form expressing the virtual work associated to the interface Γ. The physical and mathematical meaning of these forms, which may depend on $\mathbf{u}$ or other variables, will be thoroughly discussed in the next sections, for the time being it suffices to accept that (3) and (4) is a well-posed variational problem whenever the right-hand side of (3) is linear and continuous in W.

It is important to notice at this point that the time is absent from (3) and (4). This does not mean that the problem is time-independent, but rather that the time enters the mathematical problem parametrically. The surface Γ corresponds to the location of the fluid–fluid interface at some given time t, and at that time the velocity and pressure of the fluid are the unique solution to (3) and (4). Of course, since the fluid–fluid interface is a *material entity*, the interface Γ is *transported* by the fluid velocity $\mathbf{u}$ and thus evolves with time.

Remark 2.1. Notice that the time turns into a parameter because both the inertia of the fluid *and* the inertia of the interface have been neglected. The former, as is well known, would add to the left-hand side of (3) the term

$$\int_\Omega \rho \left[\frac{\partial \mathbf{u}}{\partial t} + (\mathbf{u} \cdot \nabla)\mathbf{u}\right] \cdot \mathbf{w} d\Omega,$$

while the latter would add

$$\int_\Gamma r \left[\frac{\partial \mathbf{u}}{\partial t} + (\mathbf{u} \cdot \nabla)\mathbf{u}\right] \cdot \mathbf{w} d\Gamma,$$

where r represents a superficial mass density, which could be significant for example if microscopic heavy particles are adsorbed at Γ.

Remark 2.2. If $\mathcal{P}_{\partial\Omega}$ is taken as zero, the formulation corresponds to a free-slip condition at $\partial\Omega$. As is well known, a no-slip condition does not correspond to a particular choice of $\mathcal{P}_{\partial\Omega}$ but rather to replacing the space W in the formulation by

$$W_0 \doteq \left\{\mathbf{w} \in (H^1(\Omega))^d | \mathbf{w} = \mathbf{0} \text{ at } \partial\Omega\right\}. \tag{5}$$

In this case, which is the most classical, $\mathcal{P}_{\partial\Omega}$ is identically zero on W_0.

If, further, $\mathcal{P}_\Gamma = 0$, the model considers no surface tension effects and the classical Stokes problem is recovered.

3. The virtual work of surface tension

We now derive an expression for $\mathcal{P}_\Gamma$ on the basis of energy considerations.

Consider a surface Γ at which there exists a heterogeneity in the composition or structure, leading to a corresponding energy $\mathcal{E}(\Gamma)$. Assuming this energy to be additive, it can be written as

$$\mathcal{E}(\Gamma) = \int_\Gamma \gamma(\mathbf{x}) d\Gamma, \tag{6}$$

where γ is a *surface energy density* that could depend on many variables, such as the deformation with respect to some relaxed configuration (as in elastic interfaces) or the local curvature of the interface (as in lipidic membranes), as long as γ satisfies some basic locality and objectivity principles.

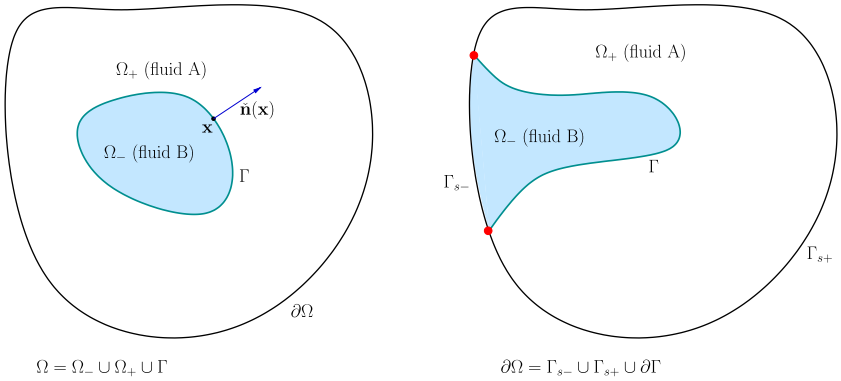

Fig. 1. Geometrical setting. On the left (respectively, right) the case without (respectively, with) triple-contact points (contact line $\partial\Gamma$ in 3D), which are represented by the red dots. (For interpretation of the references to colour in this figure legend, the reader is referred to the web version of this article.)

The simplest constitutive behavior for γ is, of course, that *the surface energy density is a constant, depending (eventually) just on the material identity of the point* $\mathbf{x}$. To further simplify the model, it can also be assumed that there is no localized dissipation at Γ. The virtual work corresponding to a velocity field $\mathbf{w}$ is thus equal to minus the rate of change of $\mathcal{E}(\Gamma)$ when Γ is virtually displaced following $\mathbf{w}$ (in other words, $-\mathcal{P}_\Gamma$ equals the *shape derivative of* $\mathcal{E}(\Gamma)$ *along the vector field* $\mathbf{w}$).

We now show that the simple model proposed above is indeed the standard surface tension model.

3.1. Computing the shape derivative

Let $\mathbf{v}$ be a vector field defined on Γ. It defines the one-parameter family of transformations

$$\boldsymbol{\varphi}_\mathbf{v} : \Gamma\times]-s_0, s_0[\to \Omega, \quad \boldsymbol{\varphi}_\mathbf{v}(\mathbf{x}, s) = \mathbf{x} + s\mathbf{v}(\mathbf{x}), \tag{7}$$

which transform Γ into the family of perturbed surfaces

$$\Gamma_{\mathbf{v},s} \doteq \{\mathbf{y} \in \Omega | \mathbf{y} = \mathbf{x} + s\mathbf{v}(\mathbf{x}), \quad \mathbf{x} \in \Gamma\}. \tag{8}$$

For s and $\mathbf{v}$ fixed, the inverse of $\boldsymbol{\varphi}_\mathbf{v}(\cdot, s)$ will be denoted by $\boldsymbol{\psi}_\mathbf{v}(\cdot, s) : \Gamma_{\mathbf{v},s} \to \Gamma$. When no confusion can arise, the subindex $\mathbf{v}$ will be omitted.

The energy of the perturbed surface $\Gamma_{\mathbf{v},s}$ is,

$$\mathcal{E}(\Gamma; \mathbf{v}, s) = \int_{\Gamma_{\mathbf{v},s}} \gamma(\boldsymbol{\psi}(\mathbf{x}, s)) d\Gamma_{\mathbf{v},s} = \int_\Gamma \gamma(\mathbf{x}) J_\Gamma(\mathbf{x}, s) d\Gamma, \tag{9}$$

where $J_\Gamma(\mathbf{x}, s) = d\Gamma_{\mathbf{v},s}/d\Gamma$ is the surface Jacobian at $\mathbf{x}$ of the transformation $\boldsymbol{\varphi}_\mathbf{v}(\cdot, s)$. Notice that $\mathcal{E}(\Gamma) = \mathcal{E}(\Gamma; \mathbf{v}, 0)$ for all $\mathbf{v}$.

These definitions allow us to define the shape derivative of $\mathcal{E}(\Gamma)$ in a precise manner as

$$d\mathcal{E}(\Gamma; \mathbf{v}) \doteq \lim_{s\to 0} \frac{\mathcal{E}(\Gamma; \mathbf{v}, s) - \mathcal{E}(\Gamma)}{s}. \tag{10}$$

We now proceed to compute this shape derivative with tools familiar to researchers in computational mechanics, namely standard continuum kinematics in 3D Cartesian coordinates. Though not in the same context, most of the tools introduced next can be found in the literature (see, for example, Chapter 2 of the book by Sokolowski & Zolésio [23]).

3.1.1. Extensions and projections

Let us define the *normal extension* of arbitrary scalar and vector fields f and $\mathbf{v}$, defined on Γ, as

$$\hat{f}(\mathbf{x}) \doteq f(\Pi_\Gamma(\mathbf{x})), \tag{11}$$
$$\hat{\mathbf{v}}(\mathbf{x}) \doteq \mathbf{v}(\Pi_\Gamma(\mathbf{x})), \tag{12}$$

where $\Pi_\Gamma(\mathbf{x})$ is the *normal projection* of $\mathbf{x}$ onto Γ. We assume Γ to be regular enough to have a well-defined normal $\check{\mathbf{n}}$ at every point, and to exist $\delta > 0$ such that to each $\mathbf{x}$ in the set

$$\mathcal{D}_\delta = \{\mathbf{x} \in \mathbb{R}^d | \mathbf{x} = \mathbf{z} + \eta\check{\mathbf{n}}(\mathbf{z}), \text{ with } \mathbf{z} \in \Gamma \text{ and } |\eta| < \delta\}, \tag{13}$$

the correspondence $\mathbf{x} \leftrightarrow (\mathbf{z}, \eta)$ is one-to-one, which allows us to define $\mathbf{z} = \Pi_\Gamma(\mathbf{x})$. See graphical explanations in Figs. 2 and 3. The definition of $\mathcal{D}_\delta$ does not require it to be contained in Ω, so that no difficulty appears if $\mathcal{D}_\delta$ intersects $\partial\Omega$.

Notice that the definition of $\hat{\mathbf{v}}(\mathbf{x})$ is made by transporting $\mathbf{v}(\Pi_\Gamma(\mathbf{x}))$ parallel to itself from the point $\Pi_\Gamma(\mathbf{x})$ to the point $\mathbf{x}$. This implies that the Cartesian components of $\hat{\mathbf{v}}(\mathbf{x})$ satisfy

$$\hat{v}_i(\mathbf{x}) = v_i(\Pi_\Gamma(\mathbf{x})). \tag{14}$$

The field $\hat{\mathbf{v}}$ can also be decomposed into **normal** and **tangential** components as

$$\hat{\mathbf{v}} = \hat{v}_n\hat{\mathbf{n}} + \hat{\mathbf{v}}_\tau, \tag{15}$$

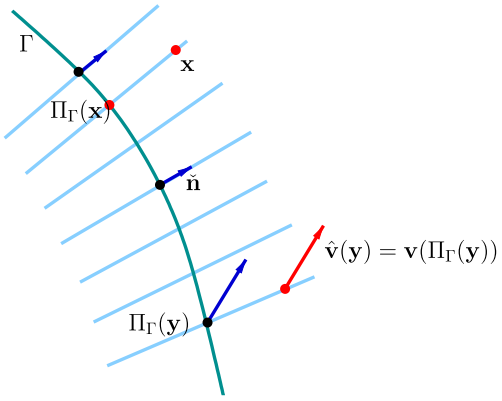

Fig. 2. Scheme defining the *normal projection* operator Π_Γ, and the *normal extension* operator $\widehat{(\cdot)}$ for the arbitrary vector field $\mathbf{v}$ defined on Γ.

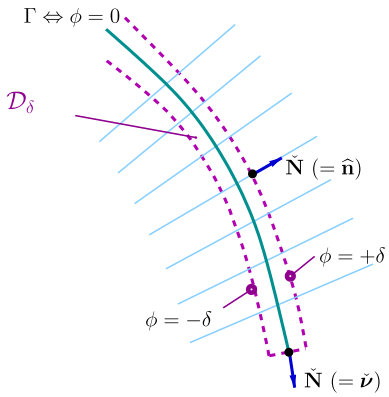

Fig. 3. Scheme defining $\mathcal{D}_\delta$, a *normal neighborhood* of Γ on which the normal extension is defined.

where $\hat{v}_n = \hat{\mathbf{v}} \cdot \hat{\mathbf{n}}$ and thus

$$\hat{\mathbf{v}}_\tau = \widehat{\mathbf{P}} \cdot \hat{\mathbf{v}} \quad (\text{in components, } (\hat{\mathbf{v}}_\tau)_i = \widehat{P}_{ij}\hat{v}_j), \tag{16}$$

where

$$\mathbf{P} = \mathbb{I} - \check{\mathbf{n}} \otimes \check{\mathbf{n}} \quad (\text{i.e.; } P_{ij} = \delta_{ij} - \check{n}_i\check{n}_j) \tag{17}$$

is the tangential projection tensor.

Remark 3.1. The normal projection coincides with the *closest-point projection*

$$\Pi_\Gamma(\mathbf{x}) = arg\, min_{\mathbf{y}\in\Gamma} \|\mathbf{y} - \mathbf{x}\|. \tag{18}$$

The latter can be viewed as a generalization of the former, since it is well defined for a wider class of surfaces. It is useful to notice the relationship between the normal projection and the signed distance function ϕ, that is,

$$\phi(\mathbf{x}) = (\mathbf{x} - \Pi_\Gamma(\mathbf{x})) \cdot \check{\mathbf{n}}(\mathbf{x}) \tag{19}$$

from which, as is well known,

$$\nabla\phi(\mathbf{x}) = \hat{\mathbf{n}}(\mathbf{x}) \tag{20}$$

and

$$\Pi_\Gamma(\mathbf{x}) = \mathbf{x} - \phi(\mathbf{x})\check{\mathbf{n}}(\Pi_\Gamma(\mathbf{x})). \tag{21}$$

3.1.2. Shape derivative

The transformation $\boldsymbol{\varphi}_\mathbf{v}$ is extended to $\mathcal{D}_\delta$ as

$$\hat{\boldsymbol{\varphi}}_\mathbf{v}(\mathbf{x}, s) = \mathbf{x} + s\hat{\mathbf{v}}(\mathbf{x}), \tag{22}$$

which is a 3D deformation to which the well-known formulae from continuum mechanics [24] apply.

Keeping $\mathbf{v}$ and s fixed and omitting them from the notation, we have, in particular (notice that the developments have been truncated to first order in s)

$$\mathbf{F} \doteq \nabla\hat{\boldsymbol{\varphi}} = \mathbb{I} + s\nabla\hat{\mathbf{v}} = \mathbb{I} + s(\hat{\mathbf{n}} \otimes \nabla\hat{v}_n + \hat{v}_n\nabla\hat{\mathbf{n}} + \nabla\hat{\mathbf{v}}_\tau), \tag{23}$$

$$\mathbf{F}^{-1} = \mathbb{I} - s\nabla\hat{\mathbf{v}} = \mathbb{I} - s(\hat{\mathbf{n}} \otimes \nabla\hat{v}_n + \hat{v}_n\nabla\hat{\mathbf{n}} + \nabla\hat{\mathbf{v}}_\tau), \tag{24}$$

$$J \doteq \det\mathbf{F} = 1 + s\nabla\cdot\hat{\mathbf{v}} = 1 + s(\hat{v}_n\nabla\cdot\hat{\mathbf{n}} + \nabla\cdot\hat{\mathbf{v}}_\tau). \tag{25}$$

Now, letting $\mathbf{dA} = \check{\mathbf{n}}d\Gamma$ denote the area differential vector and $\mathbf{da}$ its image by $\boldsymbol{\varphi}$, it is known that

$$\mathbf{da} = J(\mathbf{F}^{-1})^T\mathbf{dA} \tag{26}$$

and thus

$$\mathbf{da} = (1 + s\nabla\cdot\hat{\mathbf{v}})\mathbf{dA} - s\nabla\hat{\mathbf{v}}^T\mathbf{dA} \tag{27}$$

$$= [1 + s(\hat{v}_n\nabla\cdot\hat{\mathbf{n}} + \nabla\cdot\hat{\mathbf{v}}_\tau)]\mathbf{dA} - s\left[\nabla\hat{v}_n \otimes \hat{\mathbf{n}} + (\nabla\hat{\mathbf{v}}_\tau)^T\right]\mathbf{dA}, \tag{28}$$

where we have used $\nabla\hat{\mathbf{n}}\cdot\hat{\mathbf{n}} = 0$ ($\hat{n}_{i,j}\hat{n}_j$ is the normal derivative of $\hat{n}_i$ and is thus zero by construction of the normal extension). It can be verified that the first term on the right-hand side of (27) (or equivalently (28)) is normal to Γ, while the second term is tangential. Thus, to first order in s, since $d\Gamma_{\mathbf{v},s} = \|\mathbf{da}\|$ we have

$$d\Gamma_{\mathbf{v},s} = (1 + s\nabla\cdot\hat{\mathbf{v}})d\Gamma = [1 + s(\hat{v}_n\nabla\cdot\hat{\mathbf{n}} + \nabla\cdot\hat{\mathbf{v}}_\tau)]d\Gamma, \tag{29}$$

which combined with (9) and (10) leads to

$$d\mathcal{E}(\Gamma;\mathbf{v}) = \int_\Gamma \gamma\nabla\cdot\hat{\mathbf{v}}d\Gamma = \int_\Gamma \gamma(\hat{v}_n\nabla\cdot\hat{\mathbf{n}} + \nabla\cdot\hat{\mathbf{v}}_\tau)d\Gamma. \tag{30}$$

We now proceed to operate on this expression by integrating by parts over Γ to first arrive at the effective force distribution that the fluid exerts on the fluid, and then to derive the practical expressions that are used in numerical computations.

3.2. Surface gradients and integration by parts over surfaces

The normal extensions we have been working with allow for the definition of differential operators on surfaces without the introduction of covariant derivatives. In fact, the following definitions are equivalent to the usual ones from differential geometry.

Definition 3.2. The *surface gradient* $\nabla_\Gamma f$ of a function $f : \Gamma \to \mathbb{R}$ is the d-dimensional vector field defined by

$$\nabla_\Gamma f \doteq \nabla\hat{f}. \tag{31}$$

The *surface gradient* $\nabla_\Gamma\mathbf{v}$ of a vector field $\mathbf{v} : \Gamma \to \mathbb{R}^d$ is the rank-two tensor

$$\nabla_\Gamma\mathbf{v} \doteq \nabla\hat{\mathbf{v}}. \tag{32}$$

Finally, the tangential divergence of $\mathbf{v}$ is defined as the trace of $\nabla_\Gamma\mathbf{v}$, i.e.,

$$\nabla_\Gamma\cdot\mathbf{v} \doteq \mathrm{trace}\,(\nabla_\Gamma\mathbf{v}) = \nabla\cdot\hat{\mathbf{v}} = \hat{v}_{i,i}. \tag{33}$$

Notice that ∇_Γ is a *tangential* derivative, in the sense that $\nabla_\Gamma f\cdot\check{\mathbf{n}} = 0$ and $\nabla_\Gamma\mathbf{v}\cdot\check{\mathbf{n}} = \mathbf{0}$ (i.e.; $(\nabla_\Gamma\mathbf{v})_{ij}\check{n}_j = \hat{v}_{i,j}\check{n}_j = 0$).

A crucial role in differential geometry is played by the tensor

$$\mathbf{H} \doteq \nabla_\Gamma\check{\mathbf{n}}. \tag{34}$$

This tensor is symmetric, since

$$H_{ij} = (\nabla_\Gamma\check{\mathbf{n}})_{ij} = \hat{n}_{i,j} = (\nabla\phi)_{i,j} = \phi_{,ij}. \tag{35}$$

Further, $\check{\mathbf{n}}$ is an eigenvector of $\mathbf{H}$ with zero eigenvalue. This shows that the geometric information contained in $\mathbf{H}$ is purely tangential. Let us mention that $\mathbf{H}(\mathbf{x})$, viewed as a tensor on the tangent plane at $\mathbf{x}$, is called the *second fundamental form of* Γ **at** $\mathbf{x}$. Since $d = 3$ and one eigenvalue is necessarily zero, let us denote by $\kappa_1(\mathbf{x})$ and $\kappa_2(\mathbf{x})$ the other two eigenvalues of $\mathbf{H}(\mathbf{x})$. The **mean curvature** of Γ is defined as *the trace of* $\mathbf{H}$, that is,

$$\kappa(\mathbf{x}) \doteq \mathrm{trace}\,(\mathbf{H}(\mathbf{x})), \tag{36}$$

which also implies $\kappa = \kappa_1 + \kappa_2$ and

$$\kappa = H_{ii} = \hat{n}_{i,i} = \nabla\cdot\check{\mathbf{n}} = \nabla_\Gamma\cdot\check{\mathbf{n}}. \tag{37}$$

The mean curvature κ, being an invariant of $\mathbf{H}$, does not depend on the choice of the Cartesian frame and is thus mechanically meaningful. Also invariant is the product

$$K = \kappa_1\kappa_2, \tag{38}$$

which is the determinant of the tangential part of $\mathbf{H}$ and is known as *Gaussian curvature*. An invariant of rank-two tensors that appears frequently in mechanics is the Frobenius norm,

$$\|\mathbf{H}(\mathbf{x})\| \doteq \sqrt{\mathbf{H}(\mathbf{x}) : \mathbf{H}(\mathbf{x})} = \sqrt{H_{ij}(\mathbf{x})H_{ij}(\mathbf{x})}. \tag{39}$$

Its relationship to the invariants κ and K results from

$$\mathbf{H} : \mathbf{H} = \kappa_1^2 + \kappa_2^2 = (\kappa_1 + \kappa_2)^2 - 2\kappa_1\kappa_2 = \kappa^2 - 2K. \tag{40}$$

Remark 3.3. It is important to understand that, for a scalar field f defined not just on Γ but also defined on a neighborhood of it, and for $\mathbf{x} \notin \Gamma$, $f(\mathbf{x})$ does not in general coincide with $\hat{f}(\mathbf{x})$. In fact, $\hat{f}$ is the *normal extension of the surface values of* f and thus $\nabla f \neq \nabla_\Gamma f$.

In fact, assuming f differentiable at Γ,

$$\nabla_\Gamma f(\mathbf{x}) = \mathbf{P}(\mathbf{x})\cdot\nabla f(\mathbf{x}) \quad \mathbf{x} \in \Gamma \tag{41}$$

(in components, $(\nabla_\Gamma f)_i = P_{ij}f_j$). Similarly, for a differentiable vector field $\mathbf{v}$ defined in a neighborhood of $\mathbf{x} \in \Gamma$,

$$\nabla_\Gamma\mathbf{v}(\mathbf{x}) = \nabla\mathbf{v}(\mathbf{x})\cdot\mathbf{P}(\mathbf{x}) \quad \left(\text{i.e.; } (\nabla_\Gamma\mathbf{v})_{ij} = v_{i,k}P_{kj}\right), \tag{42}$$

which is easily proved by first noticing that, from (21),

$$\hat{\mathbf{v}}(\mathbf{x}) = \mathbf{v}(\mathbf{x} - \phi(\mathbf{x})\hat{\mathbf{n}}(\mathbf{x})) \tag{43}$$

and thus,

$$(\nabla_\Gamma\mathbf{v})_{ij} = \hat{v}_{i,j} = v_{i,k}(\delta_{kj} - \phi_{,j}\hat{n}_k - \phi\hat{n}_{k,j}),$$

which proves (42) because $\phi_{,j}(\mathbf{x}) = \check{n}_j(\mathbf{x})$ and $\phi(\mathbf{x}) = 0$.

We can now establish the integration-by-parts lemma:

Lemma 3.4. *For any f defined and differentiable on Γ,*

$$\int_\Gamma \nabla_\Gamma f d\Gamma = \int_\Gamma f\kappa\check{\mathbf{n}}d\Gamma + \int_{\partial\Gamma} f\check{\nu}d\partial\Gamma \tag{44}$$

so that, applying it componentwise, we get for any tangentially differentiable vector field $\mathbf{q}$,

$$\int_\Gamma \nabla_\Gamma\cdot\mathbf{q}d\Gamma = \int_\Gamma \kappa\check{\mathbf{n}}\cdot\mathbf{q}d\Gamma + \int_{\partial\Gamma} \check{\boldsymbol{\nu}}\cdot\mathbf{q}d\partial\Gamma, \tag{45}$$

where $\check{\mathbf{n}}$ *is the unit vector normal to* Γ *and* ν *is the unit vector tangent to* Γ *and normal to* $\partial\check{\Gamma}$ *(see Fig. 3).*

As a corollary, we have that the integral of the surface divergence of a purely tangential field on a closed surface is zero.

Proof. We use that, for any continuous function g,

$$\int_\Gamma g d\Gamma = \lim_{\delta\to 0}\frac{1}{2\delta}\int_{\mathcal{D}_\delta} g d\Omega \tag{46}$$

and integration by parts in $\mathcal{D}_\delta$, which with the definitions in Fig. 3 reads

$$\int_{\mathcal{D}_\delta} \nabla g d\Omega = \int_{\partial\mathcal{D}_\delta} g\check{\mathbf{N}}d\Gamma. \tag{47}$$

In the limit $\delta \to 0$,

$$\left(\int_\Gamma \nabla_\Gamma f d\Gamma\right)_i = \frac{1}{2\delta}\int_{\mathcal{D}_\delta}(\delta_{ij}-\hat{n}_i\hat{n}_j)\hat{f}_{,j}d\Omega = \frac{1}{2\delta}\int_{\partial\mathcal{D}_\delta}\hat{f}(\delta_{ij}-\hat{n}_i\hat{n}_j)\check{N}_j d\partial\mathcal{D} - \frac{1}{2\delta}\int_{\mathcal{D}_\delta}(\delta_{ij}-\hat{n}_i\hat{n}_j)_{,j}\hat{f}d\Omega = \int_{\partial\Gamma} f\check{\nu}_i d\partial\Gamma + \frac{1}{2\delta}\int_{\mathcal{D}_\delta}\hat{f}\hat{n}_{j,j}\hat{n}_i d\Omega \tag{48}$$

having used that $\mathbf{P}\cdot\check{\mathbf{N}}=0$ on $\phi=\pm\delta$, that $\check{\mathbf{N}}\cdot\hat{\mathbf{n}}=0$ if $\check{\mathbf{N}}=\check{\boldsymbol{\nu}}$, and that $\hat{n}_{i,j}\hat{n}_j=0$. □

3.3. Surface tension forces

Applying (45) with $\mathbf{q}=\gamma\mathbf{v}$ to (30), since

$$\gamma\nabla\cdot\hat{\mathbf{v}} = \nabla\cdot(\hat{\gamma}\hat{\mathbf{v}}) - \nabla\hat{\gamma}\cdot\hat{\mathbf{v}} = \nabla_\Gamma\cdot(\gamma\mathbf{v}) - \nabla_\Gamma\gamma\cdot\mathbf{v} \tag{49}$$

gives the following.

Proposition 3.5.

$$d\mathcal{E}(\Gamma;\mathbf{v}) = \int_\Gamma(\gamma\kappa\check{\mathbf{n}}-\nabla_\Gamma\gamma)\cdot\mathbf{v}d\Gamma + \int_{\partial\Gamma}\gamma\check{\boldsymbol{\nu}}\cdot\mathbf{v}d\partial\Gamma \tag{50}$$

so that the virtual power $\mathcal{P}_\Gamma(\mathbf{v}) = -d\mathcal{E}(\Gamma;\mathbf{v})$ *corresponds to*

- *a surface force distribution on* Γ

$$\mathbf{A} = -\gamma\kappa\check{\mathbf{n}} + \nabla_\Gamma\gamma \tag{51}$$

together with, if $\partial\Gamma\neq\emptyset$,

- *a line force distribution on* $\partial\Gamma$

$$\mathbf{T} = \gamma\check{\boldsymbol{\nu}}. \tag{52}$$

The normal part of $\mathbf{A}$ (that is, $-\gamma\kappa\check{\mathbf{n}}$) is immediately recognized as the usual *surface tension force*, and is the only effect of the surface energy if γ is constant and the surface is closed. The second part, $\nabla_\Gamma\gamma$, called *Marangoni force*, drives tangential motion of the fluid at the interface when γ varies on Γ, as happens for example as a consequence of temperature gradients (Marangoni effect).

We have thus proved that *surface tension effects correspond to variations of the energy* $\mathcal{E}(\Gamma)=\int_\Gamma\gamma d\Gamma$. This is well-known in physics but less so in mechanics, where capillary forces are in general not introduced from a variational viewpoint.

Remark 3.6. The continuity of $\mathcal{P}_\Gamma$ on $(H^1(\Omega))^d$ is immediate for the case of a closed smooth surface with smooth data. In fact, assuming Γ of class $\mathcal{C}^2$ and γ in $H^1(\Gamma)$, we have from (50) that

$$\mathcal{P}_\Gamma(\mathbf{v}) \leqslant (\kappa_{\max}+1)\|\gamma\|_{H^1(\Gamma)}\|\mathbf{v}\|_{(L^2(\Gamma))^d} \leqslant C\|\mathbf{v}\|_{(H^1(\Omega))^d}, \tag{53}$$

where $\kappa_{\max}=\max_{\mathbf{x}\in\Gamma}|\kappa(\mathbf{x})|$, and the continuity of the trace operator has been used.

For the cases in which $\partial\Gamma$ is non-empty the situation is less clear, as will be discussed later on.

An energy estimate for the continuous problem is immediate in our formulation. The time derivative of $\mathcal{E}(\Gamma)$ is clearly $d\mathcal{E}(\Gamma;\mathbf{u})$, the shape derivative in the direction of the real velocity field. Then, from (3) and (4) and assuming $\mathbf{b}$ and $\mathcal{P}_{\partial\Omega}$ to be zero for simplicity,

$$\frac{d\mathcal{E}}{dt} = d\mathcal{E}(\Gamma;\mathbf{u}) = -\mathcal{P}_\Gamma(\mathbf{u}) = -\int_\Omega 2\mu\|D\mathbf{u}\|^2 d\Omega \leqslant 0, \tag{54}$$

which proves that the energy of the system is non-increasing and, further, that the only dissipation present is the standard viscous dissipation of the bulk fluids (i.e.; surface tension forces are conservative). The proof of the same estimate by Gerbeau and Lelièvre [25] is much more involved.

Notice that $\mathbf{A}$ is not a volumetric force, but a force distribution on Γ. It is sometimes written as a singular body force $\mathbf{b}_\Gamma$ with

$$\mathbf{b}_\Gamma = (-\gamma\kappa\check{\mathbf{n}}+\nabla_\Gamma\gamma)\delta_\Gamma, \tag{55}$$

where δ_Γ stands for the surface Dirac-delta distribution. This Dirac-delta formulation is the basis of the *continuous surface force* method [26,3,27–31,6], in which the delta is regularized [32,33] and the mean curvature is numerically approximated.

In what regards the line force $\mathbf{T}$, since $\gamma(\mathbf{x})\geqslant 0$ for the fluids to be immiscible, the interface Γ is always "pulling from its boundary $\partial\Gamma$" with a force per unit length equal to γ. This explains why γ is also referred to as *surface tension* or *surface tension coefficient*.

3.4. Useful equivalent formulations for $\mathcal{P}_\Gamma$

Another approach, proposed by Bänsch [34], computes $\mathcal{P}_\Gamma(\mathbf{w})$ in (3), with $\mathbf{w}\in W$, as

$$\mathcal{P}_\Gamma(\mathbf{w}) = -\int_\Gamma\gamma\mathbf{P}:\nabla\mathbf{w}d\Gamma, \tag{56}$$

which comes from (30) and (42), since

$$\nabla_\Gamma\cdot\mathbf{w} = \nabla\cdot\hat{\mathbf{w}} = \mathrm{trace}(\nabla\mathbf{w}\cdot\mathbf{P}) = w_{i,j}P_{ji} = \mathbf{P}:\nabla\mathbf{w} = (\mathbb{I}-\check{\mathbf{n}}\otimes\check{\mathbf{n}}):\nabla\mathbf{w}. \tag{57}$$

This formulation is very appealing for finite element formulations for several reasons:

- Omitting other forces, the final variational equations for surface tension read, simply,

$$\int_\Omega 2\mu D\mathbf{u}:D\mathbf{w}d\Omega - \int_\Omega p\nabla\cdot\mathbf{w}d\Omega = -\int_\Gamma\gamma\mathbf{P}:\nabla\mathbf{w}d\Gamma, \tag{58}$$

$$\int_\Omega q\nabla\cdot\mathbf{u}d\Omega = 0. \tag{59}$$

The single term on the right of (58) accounts for the (surface-tension plus Marangoni) force $\mathbf{A}$ and the line force $\mathbf{T}$ discussed previously. Further, there is no curvature of Γ involved, just the normal vector. Though in general (58) is introduced in a way completely different to that adopted here, it has in fact been used recently by several authors in the finite element context [35–40]. The approximation error arising when W is replaced by a discrete analog W_h has been analyzed by Gross and Reusken [41]. If for some reason it is preferred to avoid the calculation of the surface integral, it can always be transformed into a volume integral by introducing the surface Dirac delta and then regularizing it [38].

- Another interesting aspect of the formulation (56) is an ingenious semi-implicit time-discretization of the capillary force that can be derived from it. This discretization was proposed by Bänsch [34], based on previous work by Dziuk and coworkers for the Laplace–Beltrami operator [42,43].

  To understand the basic idea we need to introduce the identity function

$$\boldsymbol{\chi}(\mathbf{x}) = \mathbf{x} \tag{60}$$

and denote as before $\hat{\boldsymbol{\chi}}$ the normal extension of its values on Γ. Then the following properties hold.

Lemma 3.7.

$$\hat{\boldsymbol{\chi}}(\mathbf{x}) = \Pi_\Gamma(\mathbf{x}) = \mathbf{x}-\phi(\mathbf{x})\hat{\mathbf{n}}(\mathbf{x}), \tag{61}$$

$$\nabla_\Gamma\boldsymbol{\chi} = \mathbf{P} = \mathbb{I}-\check{\mathbf{n}}\otimes\check{\mathbf{n}}, \tag{62}$$

$$\Delta_\Gamma\boldsymbol{\chi} \doteq \nabla_\Gamma\cdot\nabla_\Gamma\boldsymbol{\chi} = -\kappa\check{\mathbf{n}}. \tag{63}$$

The operator Δ_Γ in (63), defined by $\Delta_\Gamma=\nabla_\Gamma\cdot\nabla_\Gamma$, is the surface Laplacian, also called *Laplace–Beltrami* operator.

Proof. Property (61) is immediate from the definitions of Π_Γ and ϕ (the signed distance). Property (62) is proved taking the surface gradient of (61),

$$(\nabla_\Gamma \boldsymbol{\chi})_{ij} = \hat{\chi}_{i,j} = (x_i - \phi(\mathbf{x})\hat{n}_i)_{,j} = \delta_{i,j} - \phi_{,j}\hat{n}_i - \phi\hat{n}_{i,j}$$

and remembering that $\phi_{,j} = \hat{n}_j$ and that $\phi = 0$ on Γ. Finally, to prove (63), we differentiate again with respect to x_j,

$$(\Delta_\Gamma \boldsymbol{\chi})_i = (\hat{\chi}_{i,j})_{,j} = -\hat{n}_{j,j}\hat{n}_i - \hat{n}_j\hat{n}_{i,j}. \qquad \square$$

The semi-implicit treatment of $\mathcal{P}_\Gamma(\mathbf{w})$ arises thus from (putting the time step as a supra-index)

$$\begin{aligned}\int_{\Gamma^{n+1}} \gamma\mathbf{P}^{n+1} : \nabla\tilde{\mathbf{w}}d\Gamma &= \int_{\Gamma^{n+1}} \gamma\nabla_\Gamma\boldsymbol{\chi}^{n+1} : \nabla\tilde{\mathbf{w}}d\Gamma \\ &\simeq \int_{\Gamma^n} \gamma\nabla_\Gamma(\boldsymbol{\chi}^n + \Delta t\mathbf{u}^{n+1}) : \nabla\mathbf{w}d\Gamma \\ &= \int_{\Gamma^n} \gamma\mathbf{P}^n : \nabla\mathbf{w}d\Gamma + \Delta t\int_{\Gamma^n} \gamma\nabla_\Gamma\mathbf{u}^{n+1} : \nabla\mathbf{w}d\Gamma \\ &= \int_{\Gamma^n} \gamma\mathbf{P}^n : \nabla\mathbf{w}d\Gamma + \Delta t\int_{\Gamma^n} \gamma u^{n+1}_{i,k}P_{kj}w_{i,j}d\Gamma.\end{aligned}$$

The last term adds a surface Laplacian of $\mathbf{u}^{n+1}$ in the time discretization thus allowing for much larger time steps than explicit formulations while keeping the problem linear. This idea, or variants of it, has been adopted and implemented by many authors [44,38,45].

3.5. A numerical example: Marangoni effect

Let $W_h \subset W$ be the standard $\mathbb{P}_1$ element for velocity, and let $Q_h \subset Q$ be the discrete space for pressure proposed by Ausas et al. [39]. The (stabilized) discrete variational formulation of (58) and (59) reads: Find $(\mathbf{u}_h, p_h) \in W_h \times Q_h$ such that

$$\int_\Omega 2\mu D\mathbf{u}_h : D\mathbf{w}_h d\Omega - \int_\Omega p_h\nabla\cdot\mathbf{w}_h d\Omega = -\int_{\Gamma_h} \gamma\mathbf{P} : \nabla\mathbf{w}_h d\Gamma, \tag{64}$$

$$\int_\Omega q_h\nabla\cdot\mathbf{u}_h d\Omega + \int_{\Omega'} \tau_h\nabla p_h\cdot\nabla q_h d\Omega = 0 \tag{65}$$

for all $(\mathbf{w}_h, q_h) \in W_h \times Q_h$, where $\Omega' = \Omega\backslash\Gamma = \Omega^+ \cup \Omega^-$ and $\tau_h = c_\tau\frac{h^2}{\mu}$ [46–48], with $c_\tau = \frac{1}{40}$. As an additional approximation, Γ_h is defined as the zero-level set of a piecewise-linear function ϕ_h. The integral over Γ_h is performed exactly, with γ assumed constant in each element. As done in [39], the stabilization is turned off ($\tau_h = 0$) in the elements cut by the interface.

We aim to show here, by means of a numerical example, that the formulation (64) and (65) accurately accounts for both the surface tension force and the Marangoni force. Remember from (51) that the Marangoni force equals $\nabla_\Gamma\gamma$, and induces tangential motion of the fluid at the interface. Physically, non-uniformities of γ can result from a non-uniformly distributed surfactant or due, for instance, to temperature gradients (the surface tension coefficient γ decreases with increasing temperature).

The example we have chosen is the migration of an immiscible spherical droplet in an unbounded domain (in the absence of gravity) with a linear distribution for γ,

$$\gamma(\mathbf{x}) = \gamma_0 - \dot{\gamma}x, \quad \dot{\gamma} > 0. \tag{66}$$

This problem has been thoroughly studied both theoretically and experimentally in the past (see e.g. [49,50] and references therein). A sketch of the geometry and choice of coordinates can be found in Fig. 4. The corresponding differential equations and interface conditions are

$$-\mu\nabla^2\mathbf{u} + \nabla p = 0 \quad \text{on } \Omega', \tag{67}$$

$$\nabla\cdot\mathbf{u} = 0 \quad \text{on } \Omega, \tag{68}$$

$$[\![\boldsymbol{\sigma}]\!]\cdot\check{\mathbf{n}} = -\gamma\kappa\check{\mathbf{n}} + \nabla_\Gamma\gamma \quad \text{on } \Gamma \tag{69}$$

to be solved subject to the far-field conditions

$$\mathbf{u}(\mathbf{x} \to \infty) = \mathbf{0} \quad p(\mathbf{x} \to \infty) = p_\infty. \tag{70}$$

The exact solution to (67)–(70) exhibits a motion of the droplet along $+x$, with velocity

$$U = \frac{2}{15}\frac{\dot{\gamma}R}{\mu}, \tag{71}$$

which drives the interface towards regions with lower values of γ, thus reducing its energy. Let us define

$$\mathbf{v} = \mathbf{u} - U\check{\mathbf{i}}, \tag{72}$$

with $\check{\mathbf{i}}$ the unit vector along x. Then, the radial and tangential components of $\mathbf{v}$, and the pressure, can be shown to be

$$r > R\begin{cases} v_r^+ = -U\cos\theta\left(1 - \frac{R^3}{r^3}\right), \\ v_\theta^+ = U\sin\theta\left(1 + \frac{R^3}{2r^3}\right), \\ p^+ = p_\infty, \end{cases} \tag{73}$$

$$r < R\begin{cases} v_r^- = \frac{3}{2}U\cos\theta\left(1 - \frac{r^2}{R^2}\right), \\ v_\theta^- = 3U\sin\theta\left(\frac{r^2}{R^2} - \frac{1}{2}\right), \\ p^- = p_\infty + \frac{2}{R}(\gamma_0 - \dot{\gamma}r\cos\theta), \end{cases} \tag{74}$$

Notice that $\mathbf{v}$ is purely tangential at the fluid interface, i.e., the radial component is zero ($v_r^-(r = R, \theta) = v_r^+(r = R, \theta) = 0$). This implies that the shape does not change with time and thus the droplet moves at a constant velocity.

For the numerical simulations, we solve (64) and (65) using an axisymmetric 2D code, so that the horizontal coordinate is x and the vertical coordinate y is in fact the distance from the x-axis. Once $\mathbf{u}_h$ is obtained, we compute $\mathbf{v}_h = \mathbf{u}_h - U\check{\mathbf{i}}$. The computational domain is taken as $0 < x < 12R$, $0 \leqslant y < 4R$, with $R = 0.25$. It is discretized with 60,000 linear triangular elements which do not follow Γ. The approximate interface Γ_h is obtained as the zero-level set of the nodal signed distances to Γ and cuts the elements arbitrarily. We consider viscosities $\mu_A = \mu_B = 1$ and $p_\infty = 0$, and surface tension parameters $\gamma_0 = 3$ and $\dot{\gamma} = 1$. The numerical results obtained match quite well the exact solution, as shown in Fig. 5 where the numerical and exact $\mathbf{v}$-velocity contours are shown, respectively, above and below the x-axis. The velocity vectors, which are painted with the pressure field, are tangent to the droplet interface. We also show in Fig. 6 the normal and tangential components of the velocity field $\mathbf{v}_h$ on Γ, as a function of the angle θ, and compare them with the exact values $v_r(r = R, \theta) = 0$ and $v_t(r = R, \theta) = 3/2U\sin\theta$. As can be noticed in the figure, there is good

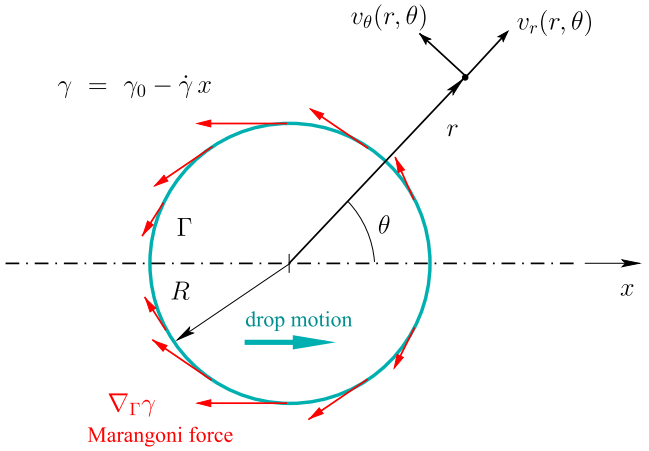

Fig. 4. Problem setting for the thermocapillary motion of a spherical droplet.

agreement between them showing that the Marangoni force is accurately accounted for.

A cross-section of the pressure field along the x-axis is plotted in Fig. 7. The pressure jump across Γ depends on the position, since $[\![p]\!] = 2\gamma/R$ and γ depends on x. This is captured by the method, as can be inferred from the left ($[\![p]\!]_\ell$) and right ($[\![p]\!]_r$) pressure jumps shown in the figure, which agree well with the exact values.

We also report an assessment of the numerical method in the three dimensional case. A mesh with 1,110,000 linear tetrahedral elements is used to discretize the computational domain $[0,3R] \times [0,2R] \times [0,2R]$. As before, the mesh does not conform to the interface. The results are in good agreement with the axisymmetrical ones, as shown in Fig. 8, where the velocity field $\mathbf{v}_h$ and its streamlines are plotted. Notice in the insert the field $\mathbf{u}_h$, the direct result of the code.

We now turn our attention to the variational formulation of problems involving contact lines.

4. Virtual work in the presence of contact lines

4.1. The basic model

The situation to consider now corresponds to the right part of Fig. 1, in which the surface Γ touches the boundary $\partial\Omega$ splitting it into a part that is in contact with fluid A (Γ_{s+}) and a part that is in contact with fluid B (Γ_{s-}). The boundary of Γ, denoted by $\partial\Gamma$, is a curve on $\partial\Omega$ which in Fig. 1 is represented by the two red dots, since it corresponds to the 2D situation.

In this setting, the changes in energy at the boundary $\partial\Omega$ when Γ moves must be considered, so that the total interface energy analogous to (6) is

$$\mathcal{E}(\Gamma) = \int_\Gamma \gamma d\Gamma + \int_{\Gamma_{s+}} \gamma_{s+} d\Gamma_s + \int_{\Gamma_{s-}} \gamma_{s-} d\Gamma_s, \tag{75}$$

where γ_{s+} and γ_{s-} denote the energy densities of the interfaces solid/fluid A and solid/fluid B, respectively. Let us denote by $\mathcal{E}_s(\Gamma)$ the sum of the second and third terms in the definition of $\mathcal{E}$ above, i.e.

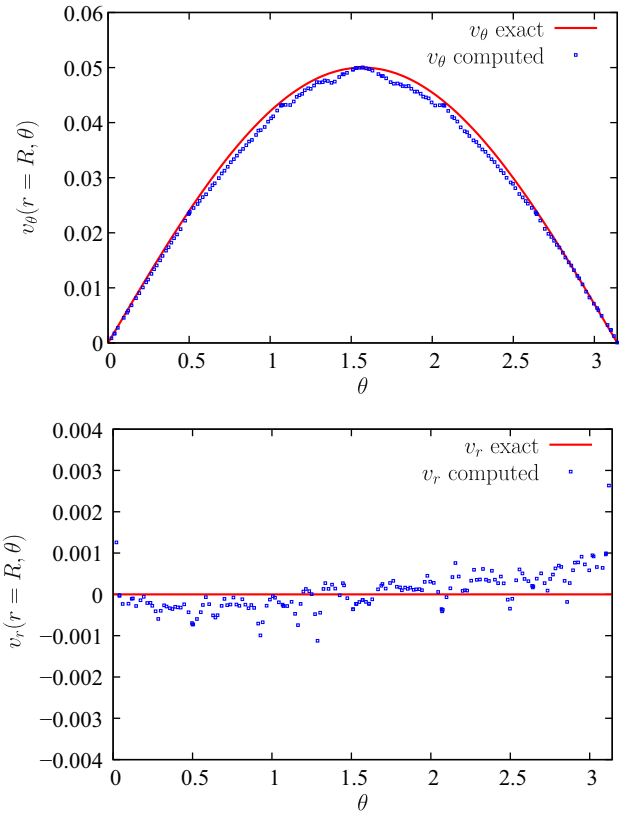

Fig. 6. Comparison of the numerical and exact normal and tangential components of the velocity field for the thermocapillary migration of a droplet.

$$\mathcal{E}_s(\Gamma) = \int_{\Gamma_{s+}} \gamma_{s+} d\Gamma_s + \int_{\Gamma_{s-}} \gamma_{s-} d\Gamma_s, \tag{76}$$

which can be obviously written as

$$\mathcal{E}_s(\Gamma) = \int_{\Gamma_{s+}\cup\Gamma_{s-}} \gamma_{s-} d\Gamma_s + \int_{\Gamma_{s+}} (\gamma_{s+} - \gamma_{s-}) d\Gamma_s. \tag{77}$$

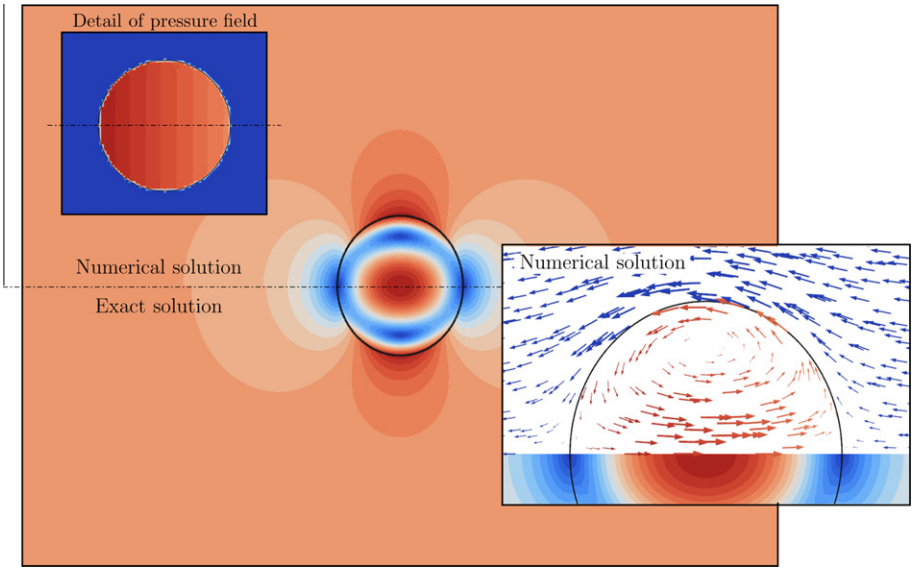

Fig. 5. Comparison of the velocity magnitude and pressure fields for the thermocapillary migration of a droplet. The solution above the symmetry line corresponds to the numerical results and the one underneath is the exact solution. The maximum in the color scale of the velocity field (red) corresponds to 0.05 and the minimum (blue) to 0. The velocity vectors are shown in the insert, with the colors corresponding to the pressure field. (For interpretation of the references to colour in this figure legend, the reader is referred to the web version of this article.)

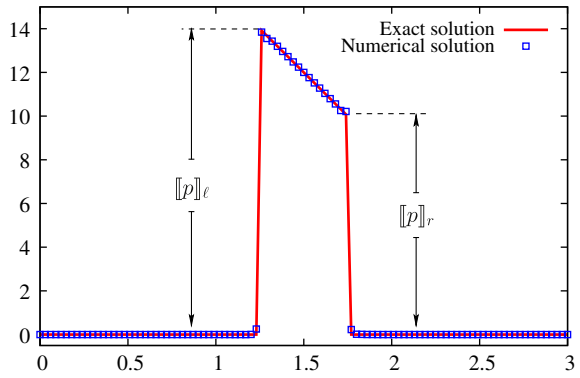

Fig. 7. Comparison of the numerical and exact pressure fields along the symmetry axis for the thermocapillary migration of a droplet.

Now, consider the geometrical definitions of Fig. 9. Assuming the solid boundary $(\Gamma_{s+} \cup \Gamma_{s-}) \subset \partial\Omega$ to be fixed, the first integral in (77) is a constant. Therefore, variations in $\mathcal{E}_s$ are only due to changes in Γ_{s+}. Applying (50) with Γ_{s+}, $\gamma_{s+} - \gamma_{s-}$ and $-\check{\mathbf{v}}_s$ playing the role of Γ, γ and $\check{\mathbf{v}}$ respectively, one obtains

$$d\mathcal{E}_s(\Gamma;\mathbf{w}) = \int_{\partial\Gamma_{s+}=\partial\Gamma} (\gamma_{s-} - \gamma_{s+})\check{\mathbf{v}}_s \cdot \mathbf{w} d\partial\Gamma, \tag{78}$$

where $\check{\mathbf{v}}_s \cdot \mathbf{w}$ is the component of $\mathbf{w}$ tangential to the solid boundary and normal to the contact line. In (78) we have used the fact that the normal component to Γ_{s+} of $\mathbf{w}$ is zero since $\mathbf{w}$ is in W (defined in (1)) and assumed γ_{s+} and γ_{s-} constants.

In the shape derivative above the fluid must slip on the surface for the contact line to move. This is contrary to the no-slip behavior that is observed away from contact lines. Another possibility would be that the interface Γ moves along Γ_s by a "rolling" motion, reminiscent of a moving tractor tread. It was experimentally proved by Dussan and Davis [51] that the kinematics of real moving contact lines indeed exhibit this kind of motion. Unfortunately, this option leads to a crucial mathematical difficulty known as *Huh and Scriven's paradox* [52] (see also [53,1,2] and the interesting discussion by Shikhmurzaev [54]). These authors proved that all solutions of the Stokes equations with no-slip conditions at the solid have infinite dissipation and thus lack physical sense. In mathematical terms, there is no velocity field in $(H^1(\Omega))^d$ satisfying $\mathbf{u} = \mathbf{0}$ on $\partial\Omega$ that is compatible with any movement of the contact line. Since contact lines indeed move, we have followed the customary treatment of relaxing the no-slip condition in the definition of W.

It would also be unphysical to assume a free-slip boundary, thus it is usual to add a Navier-type slip law at $\partial\Omega$, corresponding to a tangential force $\mathbf{t}$ proportional to $\mathbf{u}$ (i.e.; $\mathbf{t} = -\beta\mathbf{u}$). The corresponding virtual dissipation is, thus,

$$\mathcal{P}_{\partial\Omega}(\mathbf{w}) = -\int_{\partial\Omega} \beta\mathbf{u} \cdot \mathbf{w} d\partial\Omega. \tag{79}$$

Since slip is believed to take place only at molecular distances from the contact line, β is essentially $+\infty$ everywhere except in a very small vicinity of $\partial\Gamma$. In simulations, the size of this vicinity is taken as the mesh size [55]. A recent discussion of slip models and their impact on the motion of the interface Γ can be found in [56]. In the numerical examples to be shown later, however, a constant value of β was adopted to simplify the presentation.

Collecting the contributions of the fluid/solid energies γ_{s+} and γ_{s-}, and the Navier-type slip law, the right-hand side of (58) must be modified to

$$\cdots = \int_\Gamma \gamma\mathbf{P} : \nabla\mathbf{w} d\Gamma - \int_{\partial\Gamma} (\gamma_{s-} - \gamma_{s+})\check{\mathbf{v}}_s \cdot \mathbf{w} d\partial\Gamma - \int_{\partial\Omega} \beta\mathbf{u} \cdot \mathbf{w} d\partial\Omega. \tag{80}$$

We emphasize that this formulation, sometimes used in simulations [57,25], results from the shape derivative of (75) plus a standard Navier boundary condition. Though some dissipation has been added at $\partial\Omega$ through the Navier term, none has been incorporated at Γ or at $\partial\Gamma$ (the first and second integrals above are "elastic"). The lack of a concentrated dissipation at $\partial\Gamma$ has very important mechanical consequences, as detailed next.

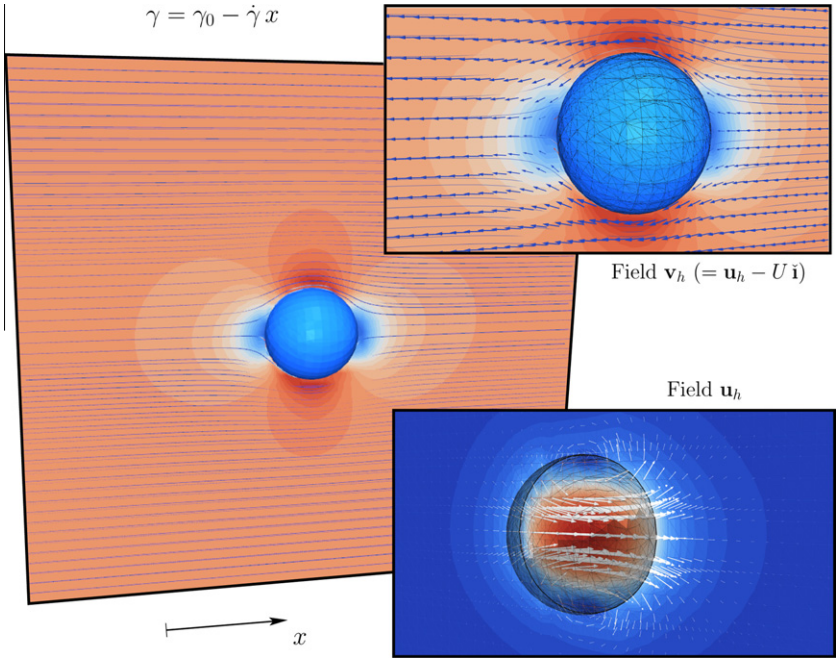

Fig. 8. Velocity field for the three dimensional simulation of the thermocapillary migration of a droplet. To provide an idea of the mesh size the reconstructed facets of Γ_h are drawn.

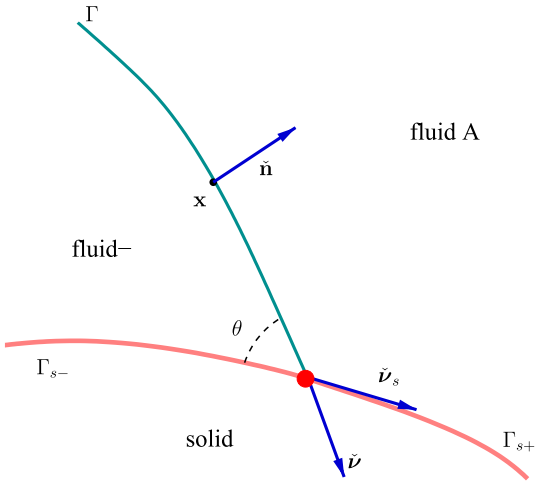

Fig. 9. Detail of the geometrical definitions near the triple contact. The contact line $\partial\Gamma$ cuts the plane of the figure perpendicularly at the red dot. (For interpretation of the references to colour in this figure legend, the reader is referred to the web version of this article.)

Proposition 4.1. *Let* $(\mathbf{u},p)\in W\times Q$ *satisfy*

$$\int_\Omega 2\mu D\mathbf{u}:D\mathbf{w}d\Omega-\int_\Omega p\nabla\cdot\mathbf{w}d\Omega = \int_\Gamma\gamma(\mathbb{I}-\check{\mathbf{n}}\otimes\check{\mathbf{n}}):\nabla\mathbf{w}d\Gamma-\int_{\partial\Gamma}(\gamma_{s-}-\gamma_{s+})\check{\boldsymbol{\nu}}_s\cdot\mathbf{w}d\partial\Gamma - \int_{\partial\Omega}\beta\mathbf{u}\cdot\mathbf{w}d\partial\Omega \tag{81}$$

for all $\mathbf{w}\in W$, *and let* $\mathbf{u}$ *also satisfy* $\nabla\cdot\mathbf{u}=0$. *Then, defining the Cauchy stress tensor*

$$\boldsymbol{\sigma}=-p\mathbb{I}+2\mu D\mathbf{u} \tag{82}$$

the following differential problem is satisfied:

$$-\nabla\cdot(-p\mathbb{I}+2\mu D\mathbf{u})=0\quad\text{on }\Omega_-\cup\Omega_+, \tag{83}$$

$$[\![\boldsymbol{\sigma}]\!]\cdot\check{\mathbf{n}}=-\gamma\kappa\check{\mathbf{n}}+\nabla_\Gamma\gamma\quad\text{on }\Gamma, \tag{84}$$

$$\mathbf{u}\cdot\check{\mathbf{n}}=0\quad\text{on }\partial\Omega, \tag{85}$$

$$\boldsymbol{\sigma}\cdot\check{\mathbf{n}}=-\beta\mathbf{u}\quad\text{on }\partial\Omega, \tag{86}$$

$$\gamma\check{\boldsymbol{\nu}}\cdot\check{\boldsymbol{\nu}}_s+\gamma_{s-}-\gamma_{s+}=0\quad\text{on }\partial\Gamma, \tag{87}$$

The proof is done by integration by parts first over Ω_+ and Ω_-, then over Γ using (45).

It must however be noticed that (81) contains, in 3D, terms of the form

$$\int_{\partial\Gamma}\mathbf{r}\cdot\mathbf{w}d\partial\Gamma$$

for some vector field $\mathbf{r}$, and in 2D of the form $\mathbf{r}(\mathbf{s})\cdot\mathbf{w}(\mathbf{s})$, where $\mathbf{s}$ is the triple point. As is well known, *these terms are not bounded in* $(H^1(\Omega))^d$. To be well defined, the test function $\mathbf{w}$ must admit a trace on $\partial\Gamma$ belonging to some $L^1(\partial\Gamma)$, which is not the case neither in 3D nor in 2D. The well-posedness of the variational problem in a $H^1(\Omega)$-setting fails, a fact that has not been pointed out in previous finite element articles on this subject [57,25,58] though it is likely to have numerical consequences. Of course, *upon discretization* all integrals in (81) are well defined whenever the discrete velocity space consists of continuous functions.

It should not be thought that the ill-posedness of (81) is a mere mathematical technicality. In a remarkable article, Dussan and Davies showed evidence that the velocity field is, in fact, (close to) multi-valued at $\partial\Gamma$ [51].

The apparent consensus is that some physical phenomenon involving a microscopic characteristic length scale ends up removing the singularity. One possibility is to modify the mathematical problem so that the interface moves with another velocity, different from $\mathbf{u}$. This approach was adopted at the discrete level by Spelt [59], who modifies the level set function so that the interface moves according to a prescribed law and at the continuous level by Shikhmurzaev [54].

Here we adopt a pragmatic viewpoint and keep assuming sufficient regularity in the involved fields for the derived expressions to make sense. The angle between Γ and Γ_s at $\partial\Gamma$ is also to be interpreted as a "macroscopic" angle, sufficiently away from the contact line to both be experimentally observable and mathematically meaningful.

Going back to the previous proposition, its most interesting part is certainly (87). Remembering the scheme in Fig. 9, one gets

$$\check{\boldsymbol{\nu}}\cdot\check{\boldsymbol{\nu}}_s=\cos\theta=\frac{\gamma_{s+}-\gamma_{s-}}{\gamma}. \tag{88}$$

Let

$$M=\frac{\gamma_{s+}-\gamma_{s-}}{\gamma}. \tag{89}$$

If $|M|\leqslant 1$ define the *static contact angle* as

$$\theta_S=\arccos\ M\quad(\text{i.e. }\gamma\cos\theta_S=\gamma_{s+}-\gamma_{s-}) \tag{90}$$

if not, $\theta_S=0$. This latter case is perfectly physical and corresponds to the **total wetting** case, in which one of the liquids spreads completely on the solid, displacing the other. The dynamics of the spreading is limited by dissipative processes near the contact line, and can be very slow.

However, by direct inspection of (88) we conclude that the basic model yields the following.

Corollary 4.2. *If* $|M|\leqslant 1$, *the interface shapes* Γ *in the variational formulation (81) make an angle* $\theta=\theta_S$ *with the solid boundary at all times. There is no "dynamic" contact angle different from the static one, since*

$$\gamma(\cos\theta-\cos\theta_S)\check{\boldsymbol{\nu}}_s=0. \tag{91}$$

If $|M|>1$, *on the other hand, the mathematical problem is not well posed.*

The previous corollary shows that the basic model above is contradictory with experiments, since the angle θ is known to depend on whether the contact line is advancing or receding, and on its velocity (see e.g. Hocking [60], Haley and Miksis [61] and references therein). The inability of the model to cope with the total-wetting situation is also a drawback. Numerical implementations yield solutions strongly dependent on the mesh, as recently shown by Afkhami et al. [62], Weinstein and Pismen [63] and Spelt [59].

It is not difficult to prove that the previous corollary still holds if inertia is incorporated in the model, be it the inertia of the fluid, or of the interface, or both.

4.2. Virtual dissipation at the contact line

One possible cure to the unphysical behaviors expressed in Corollary 4.2 is to add a localized dissipation of the form

$$\mathcal{P}_{\partial\Gamma,\text{diss}}(\mathbf{w})=\int_{\partial\Gamma}\mathbf{f}_{\text{diss}}\cdot\mathbf{w}d\partial\Gamma \tag{92}$$

to the right-hand side of the variational formulation (81). This modifies (87), or its equivalent (91), into

$$\gamma(\cos\theta-\cos\theta_S)\check{\boldsymbol{\nu}}_s+\mathbf{f}_{\text{diss}}=0 \tag{93}$$

implying that the flow will adjust so that

$$\mathbf{f}_{\text{diss}}=F\check{\boldsymbol{\nu}}_s, \tag{94}$$

where F is called *out-of-balance interfacial tension*

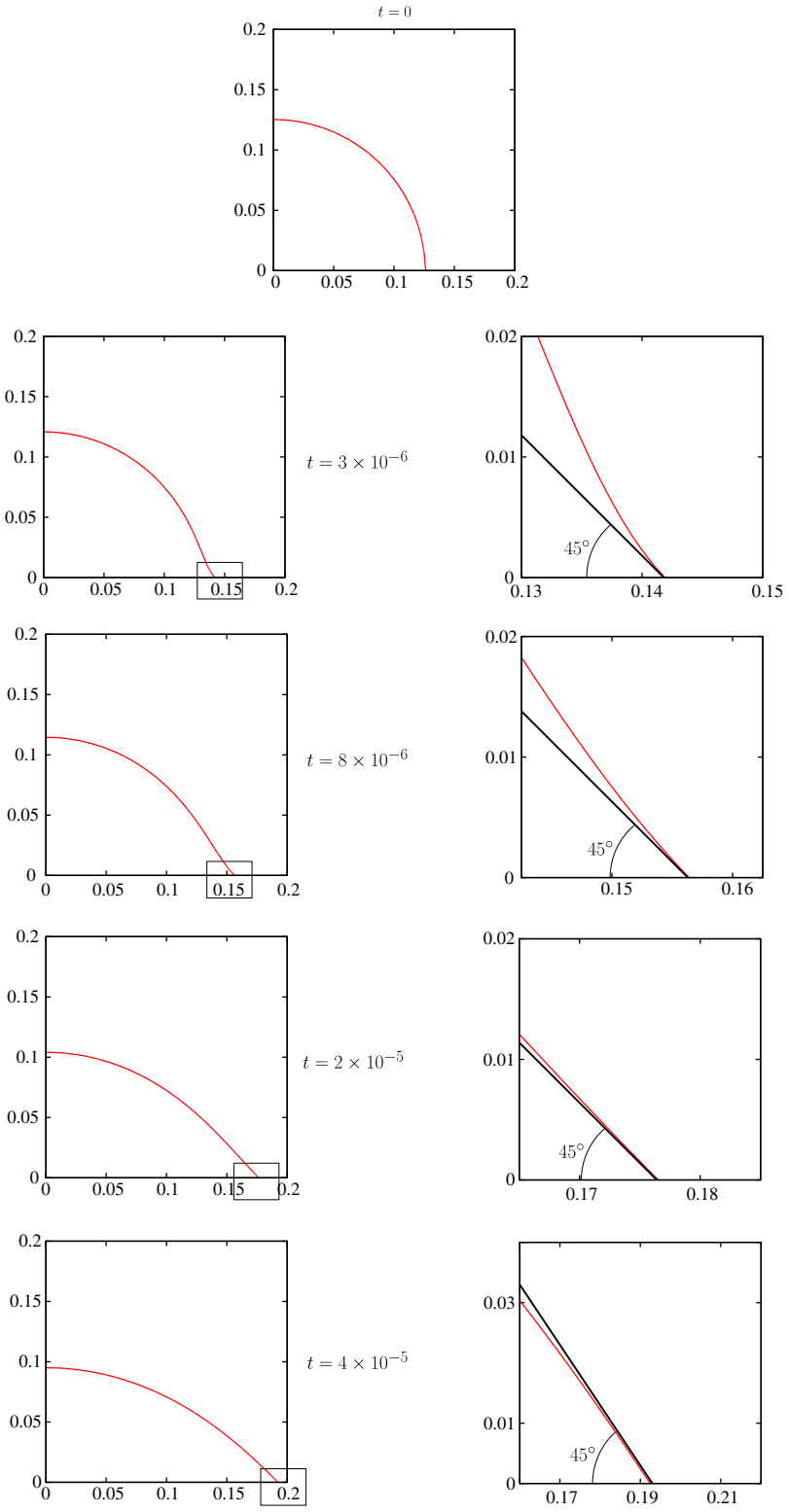

Fig. 10. Interface at different times for the spreading droplet. For each time in the right column, a detail of the interface and a straight line with 45° inclination is drawn.

$$F = \gamma(\cos\theta_S - \cos\theta). \tag{95}$$

For example, if the adopted model reads

$$\mathbf{f}_{\text{diss}} = -\zeta\mathbf{u} \tag{96}$$

a fortiori this implies that the velocity will be parallel to $\check{\mathbf{v}}_s$ and thus perpendicular to the contact line; i.e.,

$$\mathbf{u}(\mathbf{x}, t) = V(\mathbf{x}, t)\check{\mathbf{v}}_s(\mathbf{x}, t) \quad \text{for } \mathbf{x} \in \partial\Gamma(t). \tag{97}$$

Much of the physics literature in this area is devoted to understanding the relationship between F and V (or equivalently between θ and V), considering a wide variety of phenomena such as viscous dissipation, dissipation in the precursor film, activation-dominated adsorption/desorption, pinning of the contact line by defects and

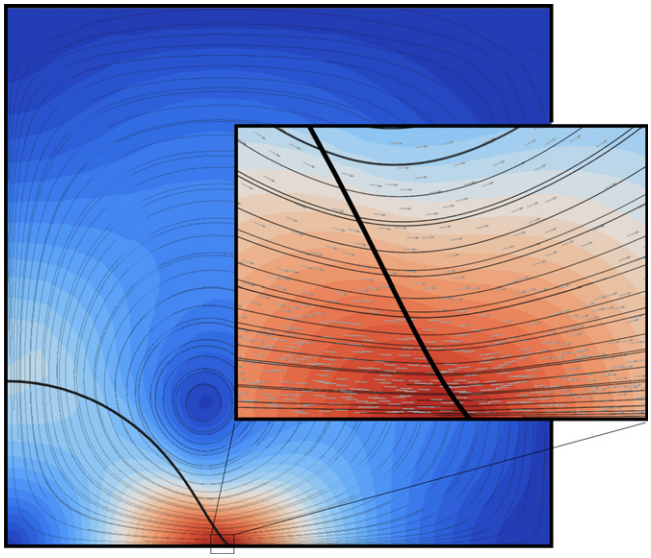

Fig. 11. Snapshot of the flow field at $t = 8 \times 10^{-6}$ for the case of Fig. 10. Velocity magnitude contours, streamlines and normalized velocity vectors. Slip coefficient β equal to 10^{-5} (corresponding to a slip length *well* resolved by the mesh) and without considering local dissipation ($\zeta = 0$). The maximum in the color scale (red) corresponds to 2673 and the minimum (blue) to 0. (For interpretation of the references to color in this figure legend, the reader is referred to the web version of this article.)

surface roughness, etc. (see [1,2,64–66] and references therein, also [67,56] for a more mechanical viewpoint). Typically, the relationship is written as

$$F = -\zeta V, \tag{98}$$

with ζ a parameter that may depend on the flow variables.

Models of contact line dissipation have seldom been used in computational fluid dynamics, but their importance is starting to be recognized. In the case of the VOF method [68], the first simulations of moving contact lines [55] assumed $F = 0$ and thus implicitly imposed the static angle. The assumption $F = 0$ was also recently adopted by Ganesan and Tobiska [57]. These authors observed that the actual contact angle $\theta(t)$ obtained from the computations differed from θ_S and related this difference to the slip parameter β. However, in view of Corollary 4.2 the continuous problem should yield $\theta(t) = \theta_S$ for all t, and any deviation from this should come from discretization errors. This will be further illustrated in the numerical example reported in the next section.

Remark 4.3. Grouping together the boundary conditions (86) and (87) one obtains, formally,

$$\boldsymbol{\sigma} \cdot \check{\mathbf{n}} + \beta \mathbf{u} + \gamma(\cos\theta - \cos\theta_S)\check{\mathbf{v}}_s \delta_{\partial\Gamma} = \mathbf{0}, \tag{99}$$

where $\delta_{\partial\Gamma}$ denotes the Dirac delta distribution along the contact line. As a consequence, Eq. (99), which has been called "Generalized Navier boundary condition" (or GNBC) in the literature [25], is another case of $F = 0$ to which Corollary 4.2 applies. Upon discretization, however, and for a suitable choice of β, the second and third terms of Eq. (99) can be made of the same order and thus lead to dynamic angles $\theta(t)$ different from θ_S. In this way the numerical computations could in principle be adjusted so as to reproduce experimental results.

The *name* GNBC, however, is in our opinion misleading. In fact, it is just a formal way of rewriting the standard Navier slip condition (86) on $\partial\Omega$ together with the contact line equilibrium condition (87), equivalent to (91) and to $F = 0$ (a "do-nothing approach").

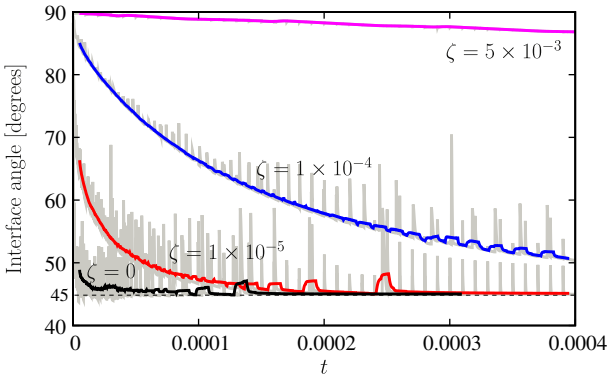

Fig. 12. Measured angle as a function of time for the spreading droplet with $\theta_S = 45°$ and different values for the constant ζ.

Manservisi and Scardovelli [58] recently discussed and implemented (in 2D) models of the form

$$F = \gamma R(\mathrm{Ca}), \quad \text{i.e.;} \quad \zeta = \frac{\gamma}{V} R(\mathrm{Ca}), \tag{100}$$

where $\mathrm{Ca} = \mu V/\gamma$ and $R(\mathrm{Ca})$ may be very simple (a power law model) or more sophisticated ones. Similarly, Afkhami et al. [62] implemented a variant of these models in which the numerical dissipation force F depends on the mesh size h. This is logical, since there will always be some part of the viscous dissipation that takes place at scales smaller than h.

Remark 4.4. In 3D, there exist two possible forms for $\mathcal{P}_{\partial\Gamma,\mathrm{diss}}(\mathbf{w})$ compatible with what has been presented above, namely

$$\mathcal{P}_{\partial\Gamma,\mathrm{diss}}(\mathbf{w}) = -\int_{\partial\Gamma} \zeta(\mathbf{u}\cdot\check{\mathbf{v}}_s)(\mathbf{w}\cdot\check{\mathbf{v}}_s) d\partial\Gamma \tag{101}$$

or

$$\mathcal{P}_{\partial\Gamma,\mathrm{diss}}(\mathbf{w}) = -\int_{\partial\Gamma} \zeta \mathbf{u}\cdot\mathbf{w} d\partial\Gamma. \tag{102}$$

The former assigns no dissipation to velocities tangential to the contact line, while the latter forces the velocity to be normal to $\partial\Gamma$. To our knowledge, it is not clear which of the previous models is to be favored in 3D simulations, though obviously the latter is simpler to implement. The final formulation for incorporating contact-line dissipation and dynamically-evolving contact angles consists simply of adding the dissipation given by (102) to the right-hand side of (81), which treated semi-implicitly would lead to an additional matrix

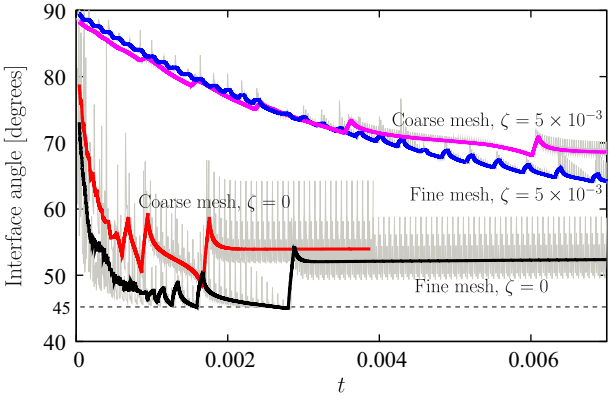

Fig. 13. Interface angle at the contact point as a function of time on a coarse mesh ($h = 5.6 \times 10^{-3}$) and a fine mesh ($h = 1.3 \times 10^{-3}$). The case without local dissipation ($\zeta = 0$) and with local dissipation ($\zeta = 5 \times 10^{-3}$) are shown.

with the structure the mass matrix of the contact line, where the line density ζ is a nonlinear function (of $\|\mathbf{u}\|$, of θ, etc.) that can possibly be updated by fixed-point iteration.

4.3. Level-set finite element method

We adopt the same stabilized finite element method of the previous section, now considering the temporal evolution of the interface. The time step size is denoted by Δt, and all variables are assumed known at time t_n, so that the unknowns correspond to time t_{n+1}. The level-set function ϕ_h belongs to the space Φ_h, which is taken as the standard $\mathbb{P}_1$ space. The time-step index appears as a supra-index. The discrete problem at each time step thus reads:

Find $(\mathbf{u}_h^{n+1}, p_h^{n+1}, \phi_h^{n+1}) \in W_h \times Q_h \times \Phi_h$ such that

$$\int_\Omega 2\mu D\mathbf{u}_h^{n+1} : D\mathbf{w}_h d\Omega - \int_\Omega p_h^{n+1} \nabla\cdot\mathbf{w}_h d\Omega = \int_{\Gamma_h^{n+1}} \gamma \mathbf{P}^{n+1} : \nabla \mathbf{w}_h d\Gamma - \int_{\partial\Gamma_h^{n+1}} (\gamma M + \zeta \check{\mathbf{v}}_s \cdot \mathbf{u}_h^{n+1}) \check{\mathbf{v}}_s \cdot \mathbf{w}_h d\partial\Gamma - \int_{\partial\Omega} \beta \mathbf{u}_h^{n+1} \cdot \mathbf{w}_h d\partial\Omega, \tag{103}$$

$$\int_\Omega q_h \nabla\cdot\mathbf{u}_h^{n+1} d\Omega + \int_{\Omega'} \tau_h \nabla p_h^{n+1} \cdot \nabla q_h d\Omega = 0, \tag{104}$$

$$\int_\Omega \left[\frac{\phi_h^{n+1} - \phi_h^n}{\Delta t} + \mathbf{u}_h^{n+1} \cdot \nabla \phi_h^{n+1} \right] \left[\psi_h + \tilde{\tau}_h \mathbf{u}_h^{n+1} \cdot \nabla \psi_h \right] d\Omega = 0 \tag{105}$$

for all $(\mathbf{w}_h, q_h, \psi_h) \in W_h \times Q_h \times \Phi_h$. Above, $\tilde{\tau}_h = \tilde{c} \frac{h}{\|\mathbf{u}_h^n\|}$ and $\tilde{c} = 0.5$, corresponding to a SUPG treatment of advection. Notice that

$$\Gamma_h^{n+1} = \{ \mathbf{x} \in \Omega | \phi_h^{n+1}(\mathbf{x}) = 0 \} \tag{106}$$

and

$$\mathbf{P}^{n+1} = \mathbb{I} - \check{\mathbf{n}} \otimes \check{\mathbf{n}} \quad \text{with } \check{\mathbf{n}} = \frac{\nabla \phi_h^{n+1}}{\|\nabla \phi_h^{n+1}\|}. \tag{107}$$

The level set is periodically reinitialized using a geometrical mass-conserving technique [69,70].

4.4. Illustrative numerical examples

Let us begin by assessing the finite element formulation (103)–(105) in the case without contact line dissipation ($F = 0$, i.e $\zeta = 0$). The parameters are set to

$$\theta_S = 45^\circ, \quad \mu_A = 10^{-5}, \quad \mu_B = 0.2 \times 10^{-6}, \quad \gamma = 0.075,$$
$$\beta = 10^{-5}, \quad \Delta t = 2 \times 10^{-7}$$

and the problem is considered two-dimensional (not axisymmetric).

The initial condition corresponds to an interface that forms an angle $\theta(t = 0) = 90^\circ$. The numerically-obtained interfaces at later times are shown in Fig. 10. On the left side of the figure the interface is plotted, while the detail of the contact point (on the right) shows that the interface assumes the static angle near the wall from the very beginning. This shows that the results of the numerical methodology are in agreement with Corollary 4.2. The last frame corresponds to the steady state shape of the droplet. A snapshot of the field variables at time $t = 8 \times 10^{-6}$ is shown in Fig. 11. The previous simulation was run on a mesh with typical mesh size $h = 1.3 \times 10^{-3}$.

In Fig. 12 we plot the contact angle as a function of time. It is clear that if $\zeta = 0$ the numerical simulation yields contact angles that are at all times equal to the static angle. The numerical contact angle was measured as the angle of the zero-level set of ϕ_h with the boundary, and exhibits some oscillations that result from the reinitialization and from the passage of the interface from one element to another.

In the same figure we also show the numerically-obtained angles for non-zero local contact-line dissipation. To simplify the presentation, three *constant* values were chosen: $\zeta = 10^{-5}$, 10^{-4} and 5×10^{-3}. In this case *dynamic* contact angles are observed, that relax towards θ_S as time evolves. No attempt has been made to tune ζ (probably as a function of $\mathbf{u}$) so as to fit some set of experimental data, since the numerical tests are oriented towards a critical assessment of the variational formulation.

It should be noticed that a length scale ℓ_β appears as a result of the Navier's boundary condition,

$$\ell_\beta = \frac{\mu_A}{\beta},$$

which in the case discussed above takes the value $\ell_\beta = 1$, so that $h \ll \ell_\beta$. In general, simulations are not able to resolve the slip length, making it important to assess the numerical method for larger values of β and coarser meshes.

Considering thus $\beta = 2 \times 10^{-2}$ (i.e.; $\ell_\beta = 5 \times 10^{-4}$), the code was run both on the previous mesh ($h = 1.3 \times 10^{-3}$) and on a coarser one ($h = 5 \times 10^{-3}$). The numerically obtained angles are shown in Fig. 13, both for $\zeta = 0$ and $\zeta = 5 \times 10^{-3}$. In agreement with other authors [57], for these underresolved cases the contact angle seems to be different from θ_S even with $\zeta = 0$. Notice however that this "dynamics" is strongly dependent on the mesh and thus a numerical artifact. With $\zeta = 5 \times 10^{-3}$, on the other hand, the dynamics of the contact angle is less mesh-dependent and thus indicative of some true underlying dynamics. The same strong mesh sensitivity of the case $\zeta = 0$ is observed for the interface position (see Fig. 14). Though the difficulty persists with $\zeta = 5 \times 10^{-3}$, it is less pronounced, thus showing the numerical advantage of adding a local dissipation at the contact line.

In Figs. 15 and 16 we show the flow variables corresponding to underresolved simulations $\beta = 2 \times 10^{-2}$ on the fine mesh ($h = 1.3 \times 10^{-3}$), for $\zeta = 0$ and $\zeta = 5 \times 10^{-3}$, respectively. The instants ($t = 7.5 \times 10^{-5}$ and $t = 3.1 \times 10^{-3}$) were chosen so that the contact line is near the position $x = 0.15$, which is also the case in Fig. 11 ($t = 8 \times 10^{-6}$).

As additional illustration, let us show that simulating the case of total wetting ($M > 1$) is also possible with this formulation. In Fig. 17 we show the evolution of a 2D droplet with a spreading parameter $M = 2$. In this case the droplet does not reach a steady state but continues spreading at a monotonously decreasing speed. Another $M = 2$ case is reported in Fig. 18. This case is three-dimensional, with an initially-prismatic shape, and was run on a mesh consisting of 480,000 tetrahedra.

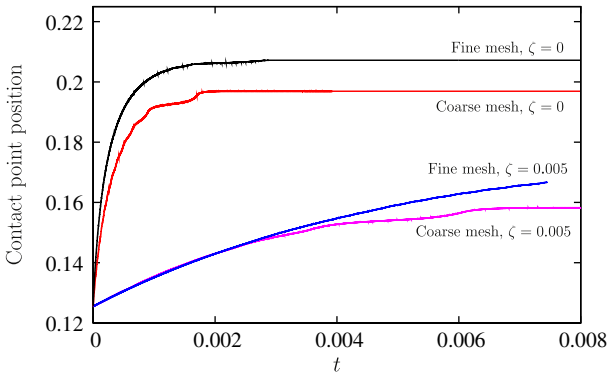

Fig. 14. Comparison of the contact point position as a function of time on a coarse mesh ($h = 5.6 \times 10^{-3}$) and a fine mesh ($h = 1.3 \times 10^{-3}$). The case without local dissipation ($\zeta = 0$) and with local dissipation ($\zeta = 5 \times 10^{-3}$) are shown.

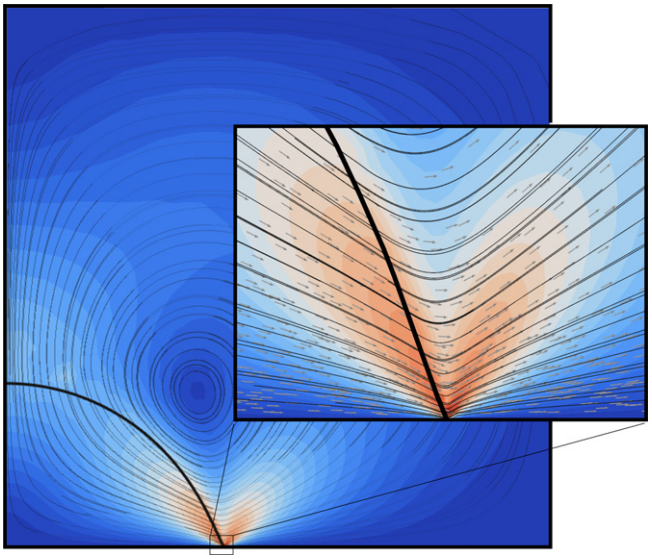

Fig. 15. Velocity magnitude contours, streamlines and normalized velocity vectors. The image corresponds to time $t = 7.5 \times 10^{-5}$ and the simulation parameters are: $\beta = 2 \times 10^{-2}$, $h = 1.3 \times 10^{-3}$ and $\zeta = 0$. The maximum in the color scale (red) corresponds to 394 and the minimum (blue) to 0. (For interpretation of the references to color in this figure legend, the reader is referred to the web version of this article.)

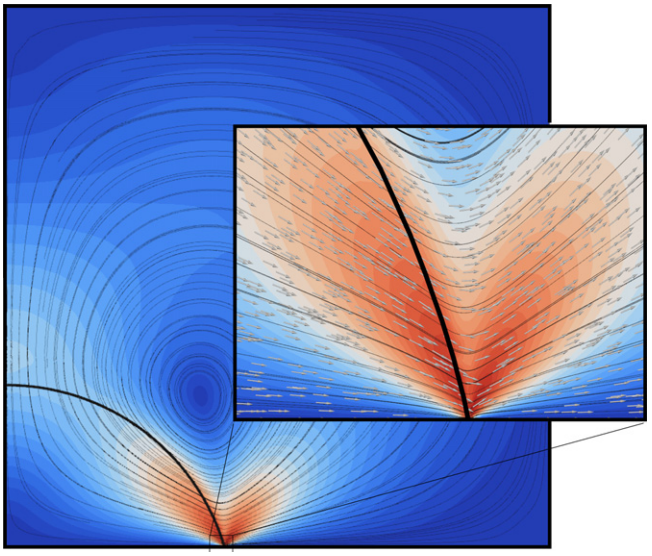

Fig. 16. Velocity magnitude contours, streamlines and normalized velocity vectors. The image corresponds to time $t = 3.1 \times 10^{-3}$ and the simulation parameters are: $\beta = 2 \times 10^{-2}$, $h = 1.3 \times 10^{-3}$ and $\zeta = 5 \times 10^{-3}$. The maximum in the color scale (red) corresponds to 7.6 and the minimum (blue) to 0. (For interpretation of the references to color in this figure legend, the reader is referred to the web version of this article.)

4.5. Imposing the contact angle in variational formulations

It has been shown that local dissipation is needed for the dynamic contact angle to differ from the static one. However, the dissipation law can be unavailable and make it preferable to impose directly the contact angle itself through a law of the type

$$\theta = \Theta(V, \ldots), \tag{108}$$

where in addition to the velocity θ may depend non-locally on material properties of the contacting media, the flow field, the geometry, etc. [53,2,71].

This imposition, in our discrete variational framework, should be viewed as a constraint and imposed by means of Lagrange multipliers. We thus have an additional unknown λ_h defined on $\partial\Gamma$ and belonging to some discrete space Λ_h. In the discrete formulation, Eq. (103) is then replaced by the following two equations:

$$\begin{aligned}\int_\Omega 2\mu D\mathbf{u}_h^{n+1} : D\mathbf{w}_h d\Omega - \int_\Omega p_h^{n+1} \nabla\cdot\mathbf{w}_h d\Omega \\ = \int_{\Gamma_h^{n+1}} \gamma \mathbf{P}^{n+1} : \nabla \mathbf{w}_h d\Gamma - \int_{\partial\Gamma_h^{n+1}} (\gamma M + \lambda_h^{n+1}) \check{\mathbf{v}}_s \cdot \mathbf{w}_h d\partial\Gamma \\ - \int_{\partial\Omega} \beta \mathbf{u}_h^{n+1} \cdot \mathbf{w}_h d\partial\Omega,\end{aligned} \tag{109}$$

$$\int_{\partial\Gamma_h^{n+1}} \eta_h [\cos\theta - \cos\Theta(\mathbf{u}_h \cdot \check{\mathbf{v}}_s)] ds = 0 \tag{110}$$

to be satisfied for all $\mathbf{w}_h \in W_h$ and $\eta_h \in \Lambda_h$. Notice that γM can be absorbed into λ_h. This can be thought equivalent to what is done by Dupont and Legendre [31] where $\mathbf{f}_{\text{diss}}$ is adjusted until the contact angle condition is satisfied, and provides a systematic extension of their method to 3D problems.

An interesting question in the previous formulation concerns the appropriate space Λ_h for the Lagrange multiplier, together with a suitable discrete evaluation of θ from the level set ϕ_h. This is a challenging open problem in this area of computational mechanics.

Further, the previous formulation does not account for contact-line pinning, for which a heuristic treatment is given in [31]. A treatment of pinning more in the spirit of (109) and (110) has been proposed recently for electrowetting in Hele–Shaw flows by Walker et al. [45].

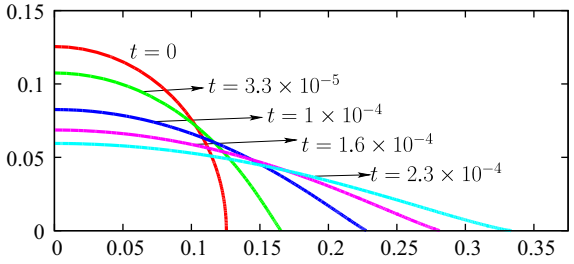

Fig. 17. Interface at different times for the spreading droplet with total wetting. Simulation parameters: $M = 2$, $\beta = 10^{-5}$, $\zeta = 10^{-4}$.

5. Concluding remarks

The purpose of this article has been to present and discuss fluid problems involving surface tension, capillarity and wetting within the framework of variational formulations, which are the usual language of computational mechanics and of finite element methods.

It has been shown how to derive the interface forces as the shape sensitivity of the interfacial energy. To avoid requiring previous knowledge of differential geometry, the required results have been proved using the embedding of Γ into $\mathbb{R}^3$ and adopting fixed Cartesian coordinates in 3D space. The static contact angle has also been shown to appear naturally from the shape sensitivity of the energy, and the necessity of adding local dissipation at the contact line to have nontrivial contact-angle dynamics has been established.

Several formulations from the literature have been derived in a unified setting so that, hopefully, some subtle difficulties inherent to this research area have been clarified. The major underlying conceptual difficulty, namely the unboundedness of $\mathcal{P}_\Gamma$ on the space W of physically-admissible velocity fields, has been explained and

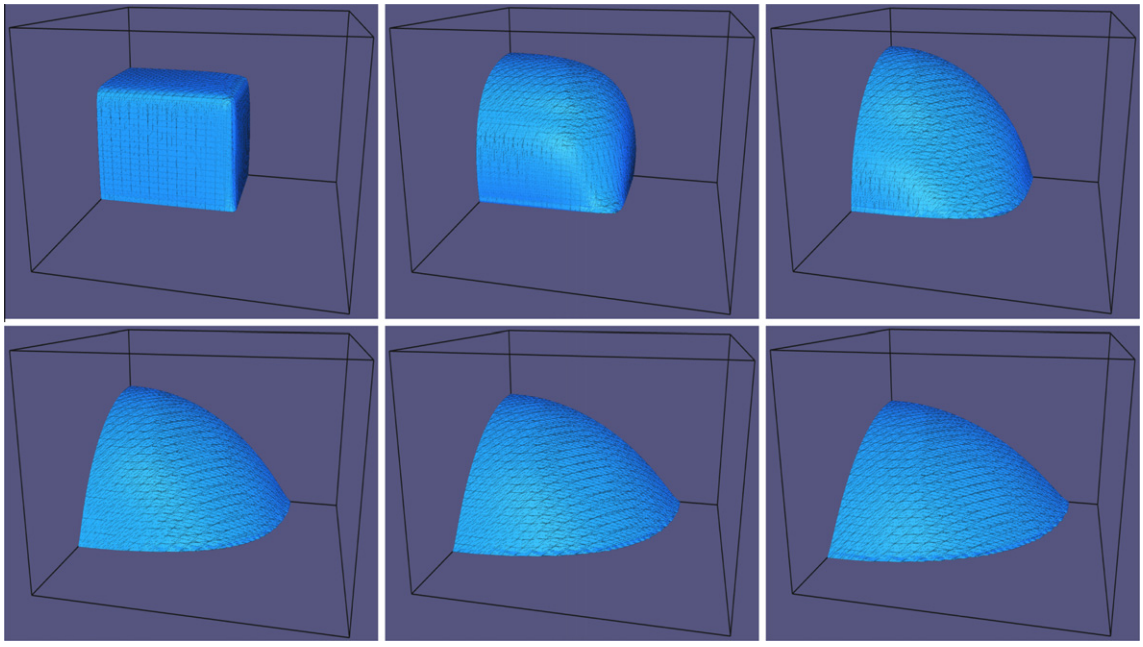

Fig. 18. Interface at different times for the spreading of an initially-prismatic droplet with total wetting. The simulation parameters are: $M = 2$, $\beta = 2 \times 10^{-2}$, $\zeta = 10^{-4}$. Shown are the times $t = 0$, 2×10^{-5}, 10^{-4}, 2×10^{-4}, 3×10^{-4} and 4×10^{-4}. Prism geometry: $(-0.125, 0.125) \times (-0.175, 0.175) \times (0, 0.125)$. Symmetry used at $x = 0$ and $y = 0$.

made evident in the variational framework (and certainly not solved). Also, some previous formulations have been extended and challenging discretization problems proposed for future research.

Acknowledgements

This work was partially supported by the Brazilian agencies CNPq and FAPESP. The support of these agencies is gratefully acknowledged. The authors thank Alexandre Carvalho, Ramon Codina, Sérgio Soares and Sergio Idelsohn for useful comments and suggestions.

References

[1] P.-G. de Gennes, F. Brochard-Wyart, D. Quéré, Capillarity and wetting phenomena, Drops, Bubbles, Pearls, Waves, Springer, 2004.
[2] D. Bonn, J. Eggers, J. Indekeu, J. Meunier, E. Rolley, Wetting and spreading, Rev. Mod. Phys. 81 (2009) 739–767.
[3] R. Scardovelli, S. Zaleski, Direct numerical simulation of free-surface and interfacial flow, Ann Rev Fluid Mech 31 (1999) 567–603.
[4] J.A. Sethian, P. Smereka, Level Set Methods for Fluids Interfaces, Ann Rev Fluid Mech 35 (2003) 341–372.
[5] T. Tezduyar, Finite elements in fluids: special methods and enhanced solution techniques, Comput. Fluids 36 (2007) 207–223.
[6] D. Fuster, G. Agbaglah, C. Josserand, S. Popinet, S. Zaleski, Numerical simulation of droplets, bubbles and waves: state of the art, Fluid Dynam. Res. 41 (2009) 065001 (24 pp.).
[7] S. Idelsohn, M. Mier-Torrecilla, E. Oñate, Multi-fluid flows with the particle finite element method, Comput. Methods Appl. Mech. Engrg. 198 (2009) 2750–2767.
[8] S. McKee, M. Tomé, V. Ferreira, J. Cuminato, A. Castelo, F. Sousa, N. Mangiavacchi, The MAC method, Comput. Fluids 37 (2008) 907–930.
[9] J. Rothstein, Slip on superhydrophobic surfaces, Ann. Rev. Fluid Mech. 42 (2010) 89–109.
[10] T. Squires, S. Quake, Microfluidics: fluid physics at the nanoliter scale, Rev. Mod. Phys. 77 (2005) 977–1026.
[11] H. Stone, A. Stroock, A. Ajdari, Engineering flows in small devices: Microfluidics toward a Lab-on-a-Chip, Annu. Rev. Fluid Mech. 36 (2004) 381–411.
[12] D. Kim, P. Wong, J. Park, A. Levchenko, Y. Sun, Microengineered platforms for cell mechanobiology, Ann. Rev. Biomed. Engrg. 11 (2009) 203–233.
[13] G. Whitesides, The origins and the future of microfluidics, Nature 442 (2006) 368–373.
[14] T. Squires, T. Mason, Fluid Mechanics of Microrheology, Ann. Rev. Fluid Mech. 42 (2010) 413–438.
[15] R. Skalak, A. Tozeren, R. Zarda, S. Chien, Strain energy function of red blood cell membranes, Biophys. J. 13 (3) (1973) 245–264.
[16] S. Marella, H. Udaykumar, Computational analysis of the deformability of leukocytes modeled with viscous and elastic structural components, Phys. Fluids 16 (2) (2004) 244–264.
[17] E. Lac, D. Barthès-Biesel, N. Pelekasis, J. Tsamopoulos, Spherical capsules in three-dimensional unbounded Stokes flows: effect of the membrane constitutive law and onset of buckling, J. Fluid Mech. 516 (2004) 303–334.
[18] C. Pozrikidis (Ed.), Modeling and Simulation of Capsules and Biological Cells, Mathematical Biology and Medicine Series, Chapman & Hall/CRC, 2003.
[19] G. Breyiannis, C. Pozrikidis, Simple shear flow of suspensions of elastic capsules, Theor. Comput. Fluid Dynam. 13 (2000) 327–347.
[20] A. Bonito, R. Nochetto, S. Pauletti, Parametric FEM for geometric biomembranes, J. Comput. Phys. 229 (2010) 3171–3188.
[21] G. Dziuk, Computational parametric Willmore flow, Numer. Math. 111 (2008) 55–80.
[22] T. Secomb, R. Skalak, Surface flow of viscoelastic membranes in viscous fluids, Quart. J. Mech. Appl. Math. 35 (1982) 233–248.
[23] J. Sokolowski, J. Zolésio, Introduction to Shape Optimization, Springer-Verlag, 1992.
[24] M. Gurtin, An Introduction to Continuum Mechanics, Academic Press, 1981.
[25] J.-F. Gerbeau, T. Lelièvre, Generalized Navier boundary condition and geometric conservation law for surface tension, Comput. Methods Appl. Mech. Engrg. 198 (2009) 644–656.
[26] J.U. Brackbill, D.B. Kothe, C. Zemach, A continuum method for modeling surface tension, J. Comput. Phys. 100 (1992) 335–354.
[27] Y. Renardy, M. Renardy, PROST: a parabolic reconstruction of surface tension for the volume-of-fluid method, J. Comput. Phys. 183 (2002) 400–421.
[28] S. Cummins, M. Francois, D. Kothe, Estimating curvature from volume fractions, Comput. Struct. 83 (2005) 425–434.
[29] M. Francois, S. Cummins, E. Dendy, D. Kothe, J. Sicilian, M. Williams, A balanced-force algorithm for continuous and sharp interfacial surface tension models within a volume tracking framework, J. Comput. Phys. 213 (2006) 141–173.
[30] S. Popinet, An accurate adaptive solver for surface-tension-driven interfacial flows, J. Comput. Phys. 228 (2009) 5838–5866.
[31] J. Dupont, D. Legendre, Numerical simulation of static and sliding drop with contact angle hysteresis, J. Comput. Phys. 229 (2010) 2453–2478.
[32] P. Smereka, The numerical approximation of a delta function with application to level set methods, J. Comput. Phys.
[33] A. Tornberg, B. Engquist, Numerical approximations of singular source terms in differential equations, J. Comput. Phys. 200 (2004) 462–488.
[34] E. Bänsch, Finite element discretization of the Navier–Stokes equations with a free capillary surface, Numer. Math. 88 (2001) 203–235.
[35] W. Dettmer, P. Saksono, D. Peric, On a finite element formulation for incompressible Newtonian fluid flows on moving domains in the presence of surface tension, Commun. Numer. Meth. Engrg. 19 (2003) 659–668.
[36] P. Saksono, D. Peric, On finite element modelling of surface tension: variational formulation and applications – Part I: Quasistatic problems, Comput. Mech. 38 (2006) 265–281.
[37] P. Saksono, D. Peric, On finite element modelling of surface tension: Variational formulation and applications – Part II: Dynamic problems, Comput. Mech. 38 (2006) 251–263.
[38] S. Hysing, A new implicit surface tension implementation for interfacial flows, Int. J. Numer. Meth. Fluids 51 (2006) 659–672.

[39] R. Ausas, F. Sousa, G. Buscaglia, An improved finite element space for discontinuous pressures, Comput. Methods Appl. Mech. Engrg. 199 (2010) 1019–1031.
[40] S. Gross, A. Reusken, An extended pressure finite element space for two-phase incompressible flows with surface tension, J. Comput. Phys. 224 (2007) 40–58.
[41] S. Gross, A. Reusken, Finite element discretization error analysis of a surface tension force in two-phase incompressible flows, SIAM J. Numer. Anal. 45 (2007) 1679–1700.
[42] G. Dziuk, An algorithm for evolutionary surfaces, Numer. Math. 58 (1991) 603–611.
[43] G. Dziuk, C. Elliott, Finite elements on evolving surfaces, IMA J. Numer. Anal. 27 (2006) 262–292.
[44] E. Bänsch, P. Morin, R. Nochetto, A finite element method for surface diffusion: the parametric case, J. Comput. Phys. 203 (2005) 321–343.
[45] S. Walker, A. Bonito, R. Nochetto, Mixed finite element for electrowetting on dielectric with contact line pinning, Interf. Free Bound. 12 (2010) 85–119.
[46] T. Hughes, L. Franca, M. Balestra, A new finite element formulation for computational fluid dynamics: V. Circumventing the Babuška–Brezzi condition: a stable Petrov–Galerkin formulation of the Stokes problem accommodating equal-order interpolations, Comput. Methods Appl. Mech. Engrg. 59 (1986) 85–99.
[47] R. Codina, A stabilized finite element method for generalized stationary incompressible flows, Comput. Methods Appl. Mech. Engrg 190 (2001) 2681–2706.
[48] R. Codina, J. Blasco, G. Buscaglia, A. Huerta, Implementation of a stabilized finite element formulation for the incompressible Navier–Stokes equations based on a pressure gradient projection, Int. J. Numer. Meth. Fluids 37 (2001) 410–444.
[49] N. Young, J. Goldstein, M. Block, The motion of bubbles in a vertical temperature gradient, J. Fluid Mech. 6 (1959) 350–356.
[50] R. Balasubramaniam, An-Ti Chai, Thermocapillary migration of droplets: an exact solution for small Marangoni numbers, J. Colloid Interf. Sci. 119 (1987) 531–538.
[51] E. Dussan, S. Davis, On the motion of a fluid–fluid interface along a solid surface, J. Fluid Mech. 65 (1974) 71–95.
[52] C. Huh, L. Scriven, Hydrodynamic model of steady movement of a solid/liquid/fluid contact line, J. Colloid Interf. Sci. 35 (1971) 85–101.
[53] E. Dussan, On the spreading of liquids on solid surfaces: static and dynamic contact lines, Ann. Rev. Fluid Mech. 11 (1979) 371–400.
[54] Y. Shikhmurzaev, Singularities at the moving contact line. Mathematical, physical and computational aspects, Physica D 217 (2006) 121–133.
[55] M. Renardy, Y. Renardy, J. Li, Numerical simulation of moving contact line problems using a Volume-of-Fluid method, J. Comput. Phys. 171 (2001) 243–263.
[56] W. Ren, W. E, Boundary conditions for the moving contact line problem, Phys. Fluids 19 (2007) 022101.
[57] S. Ganesan, L. Tobiska, Modelling and simulation of moving contact line problems with wetting effects, Comput. Visual. Sci. 12 (2009) 329–336.
[58] S. Manservisi, R. Scardovelli, A variational approach to the contact angle dynamics of spreading droplets, J. Comput. Phys. 38 (2009) 406–424.
[59] P. Spelt, A level-set approach for simulations of flows with multiple moving contact lines with hysteresis, J. Comput. Phys. 207 (2005) 389–404.
[60] L. Hocking, Sliding and spreading of thin two-dimensional drops, Q. J. Mech. Appl. Math. 34 (1981) 37–55.
[61] P. Haley, M. Miksis, The effect of the contact line on droplet spreading, J. Fluid Mech. 223 (1991) 57–81.
[62] S. Afkhami, S. Zaleski, M. Bussmann, A mesh-dependent model for applying dynamic contact angles to VOF simulations, J. Comput. Phys. 228 (2009) 5370–5389.
[63] O. Weinstein, L. Pismen, Scale dependence of contact line computations, Math. Model. Natural Phenom. 3 (2008) 98–107.
[64] M. de Ruijter, J. De Coninck, G. Oshanin, Droplet spreading: partial wetting regime revisited, Langmuir 15 (1999) 2209–2216.
[65] S. Semal, T. Blake, V. Geskin, M. de Ruijter, G. Castelein, J. De Coninck, Influence of surface roughness on wetting dynamics, Langmuir 15 (1999) 8765–8770.
[66] D. Seveno, A. Vaillant, R. Rioboo, H. Adão, J. Conti, J. De Coninck, Dynamics of wetting revisited, Langmuir 25 (2009) 13034–13044.
[67] R. Cox, The dynamics of the spreading of liquids on a solid surface. Part 1. Viscous flow, J. Fluid Mech. 168 (1986) 169–194.
[68] C. Hirt, B. Nichols, Volume of fluid (VOF) method for the dynamics of free boundaries, J. Comput. Phys. 39 (1981) 201–225.
[69] F. Mut, G. Buscaglia, E. Dari, New mass-conserving algorithm for level set redistancing on unstructured meshes, J. Appl. Mech. 73 (2006).
[70] R. Ausas, E. Dari, G. Buscaglia, A geometric mass-preserving redistancing scheme for the level set function, Int. J. Numer. Methods Fluids 65 (2010) 989–1010.
[71] A. Lukyanov, Y. Shikhmurzaev, Effect of flow field and geometry on the dynamic contact angle, Phys. Rev. E 75 (2007) 051604.